How does your gyroid grow? A mesoatomic perspective on supramolecular, soft matter network crystals

Gregory M. Grason[1,*] and Edwin L. Thomas[2]
[1]Department of Polymer Science and Engineering, University of Massachusetts, Amherst, Massachusetts 01003, USA
[2]Department of Materials Science and Engineering, Texas A & M University, College Station, Texas 77843, USA

(Received 30 November 2022; revised 20 February 2023; accepted 16 March 2023; published 21 April 2023)

We propose and describe a framework to understand the structure of supramolecular network crystals formed in soft matter in terms of mesoatomic building blocks, collective groupings of amphiphilic molecules that play a role analogous to atomic or molecular subunits of hard matter crystals. While the concept of mesoatoms is intuitive and widely invoked in crystalline arrangements of spherelike or cylinderlike (micellelike) domains, analogous notions of natural and physically meaningful building blocks of triply periodic network (TPN) crystals, like the double-gyroid or double-diamond structures are obscured by the complex, bicontinuous domain shapes and intercatenated topologies of the double networks. Focusing on the specific example of diblock copolymer melts, we propose generic rules for decomposing TPN crystals into a unique set of mesoatomic building blocks. Based on physically motivated principles, the combination of symmetries and topologies of these structures point to mesoatomic elements associated with the nodal connections, leading to mesoatomic volumes that are nonconvex and bound by smoothly curved faces, unlike the more familiar Voronoi polyhedral shapes associated with spherelike and cylinderlike mesoatoms. We analyze the shapes of these mesoatoms, their internal structure, and importantly, their local packing with neighbor mesoatomic units. Importantly, we hypothesize that mesoatoms are kinetically favored intermediate structures whose local shapes and packing template network crystal assembly on long time scales. We propose and study a minimal energetic model of mesoatom assembly for three different cubic double-network crystals, based on local shape packing, which predicts a detailed picture for kinetics of intercatenation and surface growth. Based on these analyses, we discuss several possible extensions and elaborations of the mesoatomic description of supramolecular soft matter network crystals, most notably the implications of mesoatomic malleability, a feature that distinguishes soft matter from hard matter crystals. We describe experimental observations of malleable mesoatomic units in the precursor sponge phase as well as in ordered cubic networks and suggest possibilities for observing mesoatoms in primordial, precrystalline states.

DOI: 10.1103/PhysRevMaterials.7.045603

I. INTRODUCTION

Supramolecular assembly into long-range ordered soft crystals occurs for nearly every class of soft molecular assembly, from surfactants in water [1] and liquid crystals to block copolymers (BCPs) [2] and so-called giant amphiphiles [3]. Paradigmatic examples of this are the micellar lattice phases of amphiphilic molecules [4]. Local segregation between chemically immiscible regions on the same molecule, caused by both repulsive and attractive local forces, drive the aggregation of groupings of molecules, as mismatch between local shapes of distinct parts of the molecule, possibly in combination with affinity for solvent exposure, can favor curvature of the interface between those distinct molecular regions favoring, for example, cylindrical or spherical micelle aggregates. In neat systems, or at high enough concentrations in solvated systems, the micellar units strongly interact [5,6], leading to the formation of periodically ordered equilibrium states. In these ordered states, micellar groupings of molecules are situated in crystalline arrangements [e.g., body-centered cubic (BCC) or face-centered cubic (FCC) lattices] [7–9], and hence, an individual micelle can be thought of as a *mesoatom*[1], analogous to the atomic units that serve as the building blocks of solid-state crystals.

Broadly speaking, this mesoatomic perspective has been highly valuable for two key reasons. For one, assessing the geometry of mesoatomic volumes based on space-filling tessellations of the crystal packing has enabled rational frameworks for understanding thermodynamic selection of the crystal symmetry. For example, a common heuristic approach is to assume that spherelike mesoatoms are deformed to conform to polyhedral, Voronoi-like partitions that bound the occupied Wyckoff sites and then to compare different

*grason@umass.edu

[1]To our knowledge, soft matter "mesoatoms" were first invoked in a slightly different context of symmetry-programmed colloidal particles by Shin, Bowick, and X. Xing [10].

measures of geometric distortion relative to ideal spherical shapes (e.g., minimal area) [11–15]. Rational arguments and theories along these lines predict, for example, that under certain conditions, canonical simple crystal packings like BCC become unstable to surprising and much lower symmetry structures, like Frank-Kasper crystals [16–20]. Beyond equilibrium states, the mesoatomic picture has obvious implication for kinetics and transformation pathways to soft crystal formation, in which aggregation of mesoatomic units themselves are the primary step in the hierarchical pathway for the ultimate structure formation followed by the subsequent binding and rearrangement of mesoatoms into crystalline arrays taking place on a much longer time scale. Hence, the structure and collective behavior of mesoatomic intermediates has a critical impact on the time scales that soft crystal structures form (i.e., nucleation and growth) as well as on the nature of defects present in the structures. Moreover, in most systems, soft crystals are formed by controlled quenches from a lower concentration and/or higher temperature, and hence, the conditions at which mesoatomic units are born are in general quite different from the final state of the material, which is often solvent free. The pathway dependence gives rise to rich possibilities for creating long-lived, essentially frozen, out-of-equilibrium states, with symmetries that are distinct from the more limited palette of purely equilibrium states.

While the picture is intuitive for periodic assemblies of convex and discretely defined domain shapes (e.g., spheres and cylinders), the basic notion of a mesoatomic unit is confounded by a whole class of supramolecular crystals, namely, triply periodic networks (TPNs), sometimes called bicontinuous phases. These are most often cubic phases that form at conditions that are intermediate to lamellar or cylindrical domain shapes [1], in which the domains themselves are continuous and topologically intercatenated throughout the bulk structure. Two canonical examples are the double-gyroid (DG) and double-diamond (DD) phases, which in the simplest cases are composed of two types of subdomain: the inner region (usually minority component) of interconnecting tubular domains (3- and 4-valent nodal connections for DG and DD, respectively) separated by a slablike matrix domain, whose undulating shape roughly approximates a triply periodic minimal surface (TPMS), known as gyroid and diamond minimal surfaces for DG and DD, respectively [21,22]. The tubular phases of DG and DD form two intercatenated networks: The respective tubular networks of DG and DD interlink in 10- and 6-member links (i.e., 10,3 and 6,4 nets).

The complex structures of TPN crystals are highly attractive and long sought after for a range of functional material applications due to the high volumetric surface areas afforded by their intermaterial dividing surfaces (IMDSs) and polycontinuous domain topologies [23]. However, numerous basic questions remain about how and why they form. In the context of the mesoatomic paradigm summarized above, it is unclear what the elementary building blocks of TPN crystals are since the simplest notions of domain would imply that each bulk structure contains only two domains (i.e., the subnetworks) containing an extensive number of links between them. Hence, the kinetically accessible pathways that guide the combination of long-range positional order and topological domain connectivity of TPN crystals are not presently known, nor is it clear whether these correspond to characteristic groupings of molecules and how these relate to the ultimate structures.

In this paper, we propose and outline a mesoatomic construction for understanding the structure of TPN crystals of supramolecular soft matter crystals. Our discussion is primarily centered on the specific case of diblock copolymer melts as a paradigmatic example of a TPN-forming system, although it can be understood that this perspective extends to other classes of soft-molecular building blocks, not to mention more complex BCP systems. Here, we propose some elementary principles that guide the definition of the mesoatomic building blocks of network crystals. We show how these mesoatomic units can be defined as the nonconvex analogs to the Voronoi-like polyhedra that tesselate crystals composed of spherelike domains. In the case of TPN crystals of AB amphiphiles (e.g., diblocks), mesoatoms are associated with high-symmetry nodal regions of the network morphologies and, unlike polyhedral (e.g., Voronoi) cells, are bounded by positively and negatively curved (saddle-shaped) faces as well as (approximately) planar faces. We describe the structure of canonical TPN crystals, including DG, DD, and double-primitive (DP) structures, in terms of the local packing of mesoatomic clusters and the topology of the networks these units form. Next, we consider a simple model in which contact between shape-complementary neighbors templates the assembly, growth, and intercatenation of the TPN crystals and ultimately guides larger length-scale morphological features such as surface faceting. We also discuss the experimental context for the observations and implications of the mesoatom concept in BCPs. Finally, we outline a series of open questions posed by and possible extensions to the mesoatomic hypothesis for the formation and properties of TPN crystals.

II. DEFINING THE MESOATOM

Here, we outline the principles for defining and extracting the mesoatomic building blocks of TPN crystals. Our definition specializes to the case of linear AB diblock copolymer melts, as a prototypical example. In this system, ordered phases consist of uniformly filled but molten (i.e., solvent free but fluid) packing of brushlike subdomains of chemically distinct A- and B-type polymer chains, covalently joined at their junctions, which are localized to two-dimensional (2D) IMDSs that separate the unlike brush subdomains [2,24]. In the discussion that follows, we outline possibilities and challenges to extending this paradigm to other molecular systems that form these structures. As a starting point, we assume correct knowledge of the crystallographic space group of the final crystal, the shapes and topologies of the A and B domains, and the basic model of how the chains are packed in those domains. Notably, the first two of these three descriptors can be measured by careful experimentation (except for more realistic deviations from idealized crystallographic order), while the last is currently essentially invisible to experimental characterization. Hence, the expected chain trajectories rely on information from computational models as well as heuristic assumptions about likely chain trajectories (as discussed in detail in Ref. [25]).

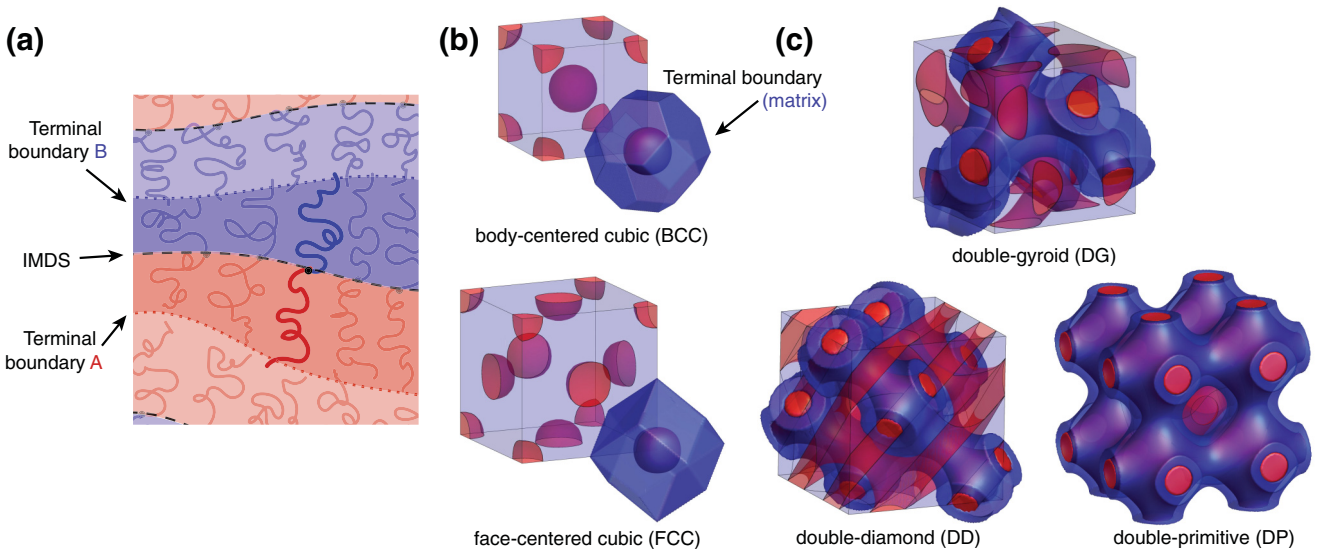

FIG. 1. Domain anatomy of block copolymer crystal phases. (a) Schematic illustration of subdomain packing of linear diblock copolymer chains in melt domains, where a single domain is defined as a set of chains whose A-B junctions are associated with a particular intermaterial dividing surface (IMDS; darker blue and red melt regions corresponding to a single domain of the quasilamellar geometry). (b) Putative shape of compact spherelike domains (darkened red volumes) surrounded by a blue outer volume with the expected faceting of the outer terminal boundaries separating neighboring spherelike mesoatom domains. (c) Single mesoatom domains of double-network crystals. Unlike the sphere case, due to network connectivity, there are only two domains in the entire volume (one for each network).

To begin with, we clarify our objective in terms of the arguably much more intuitive case of crystals of spherical or cylindrical domains. In this case, one can break these structures into micellar (i.e., spherical or cylindrical) building blocks, which when packed together become warped into lower-symmetry polyhedral volumes. Beyond being the structural elements of the ultimate crystal, such micellar mesoatoms are often understood as kinetic intermediates, forming first into spherical or cylindrical groups and then over longer time scales organizing into long-range ordered and densely packed crystals [26,27]. In this context, we clarify our intended notion of mesoatoms of a more general class of supramolecular crystals, which are not necessarily composed of convex quasispherical or quasicylindrical molecular groupings. That is, more generally, we aim for a notion of mesoatoms as groups of molecules that act collectively as building blocks of a supramolecular structure and which can be identified from the ultimate crystalline structure (akin to the Voronoi-like polyhedral volumes for quasispherical domains, see, e.g., BCC and FCC structures in Fig. 1). Ideally, the packing and deformation of mesoatoms should be useful to describe the behavior of the crystalline structure as a whole. Further, so-defined mesoatoms should represent likely kinetic intermediates whose structure and organization form the basis to understand how the crystal structure forms and evolves toward its final mature state.

Before proceeding to construct the mesoatoms of TPN phases, it is important to point out that the notion of *shape malleability* is fundamental to their properties. While BCP and other supramolecular systems may favor specific local geometries, it should be recognized that free energy differences between distinct local motifs can be fairly small compared with the relevant thermal energy. Hence, shape distortions away from idealized symmetries, as well as polymorphism between distinct symmetries, will be essential to their physical behavior. Moreover, malleability implies that the shapes and packing of mesoatomic groups into distinct periodic arrangements are intrinsically coupled, a notion that has recently gained currency in the context of complex crystals of soft spherical mesoatomic assemblies (e.g., Frank-Kasper phases) [13].

To understand the complexity of defining a useful notion of mesoatoms for TPN phases, we briefly review the anatomy of the DG crystal of diblocks as a concrete example. The DG is a cubic network morphology with $Ia\bar{3}d$ space group symmetry [28,29]. In diblock melts, it is composed of two tubular network regions, usually the minority component (say, the A block), separated by a matrix B-block layer. The IMDSs then have the shape of a tubular surface that interconnects the 3-valent nodes. The nodes of the distinct networks, each of which can be considered a single gyroid (SG), are centered on Wyckoff positions 16*b*. The nodes of one SG network correspond to 8 of the 16*b* sites (specifically, these are either 8*a* or 8*b* positions of the $I4_132$ subgroup), while the 8 nodes of the second network are given by inverting the first network through the center of the unit cube. For DG, each of the SG networks is chiral, with a handedness that can be associated with the dihedral rotation between neighboring nodes [30]. For this paper, we refer to the alternate single networks of the double-network crystals as + or −, independent of whether the network is chiral.

As we describe below, the notion of mesoatoms is intimately connected to the concept of a *domain* in the BCP melts, following the topological definitions introduced in Ref. [25]. Simply put, a domain corresponds to the volumes occupied by chains that have their junctions located on or associated with a particular IMDS. Hence, each domain is a type of double layer of A and B brushes, separated by the IMDS

containing their common junctions. This domain decomposition, by necessity, introduces a second set of boundaries at the outer and inner edges of the domain, referred to as the *terminal boundaries*. The terminal boundaries are the dividing points between brush domains of the same chemistry: A segment at the terminal boundary has equal probability to associate with at least two distinct IMDSs (or IMDS positions). Colloquially, the terminal boundary can be thought of as the contact surface between two opposing brushlike subdomains, each of which stems from the IMDS of distinct domains. Given this notion, it has been proposed that the terminal boundary is well approximated by *medial sets* of the IMDSs [25,31,32], which are loci of midpoints within a region of the A or B component between distinct IMDS regions. For the DG network, the outer terminal surface that separates the two networks closely approximates the gyroid minimal surface, and the corresponding boundary for DD and DP closely match the Schwarz D and P minimal surfaces, respectively [33].

In this context, the DG includes exactly 2 domains, one for each of the SG networks (which are enantiomeric), and the outer terminal boundary that separates them in the middle of the B matrix is a close approximation to Schoen's G minimal surface [34]. Note that, for the crystal packings of spherelike and cylinderlike domains [e.g., Fig. 1(b)], each domain corresponds to a single compact mesoatom, whereas in the double-network crystals like DG, DD, and DP, only 2 constituent domains span the entire volume of the crystal. Figure 1(c) shows examples of these macroscopic network domains for DG, DD, and DP in contrast to the compact discrete shapes of the crystalline packings of spherical domains. As topologically well-defined objects, the 2 single-network domains of these double-network morphologies are natural groupings of molecules.

However, for the purposes of the mesoatomic construction, single-network domains are obviously problematic. First, each is macroscopically large, spanning the entire volume, and second, the two networks in the final morphology are topologically intercatenated. Simply put, there is no way for two preformed single-network domains to interlink into the final double network without a (kinetically prohibitive) process of a multitude of breaking and relinking events. Note that this topological problem of interlinked domains is not encountered for quasispherical or quasicylindrical domains, where each domain (corresponding to each spherical or cylindrical IMDS) constitutes a single convex mesoatomic unit. From this perspective, it may now be intuitive to see that mesoatoms need to be defined as *prelinked* (i.e., not yet linked) subelements of these single-network domains. Next, we ask, what is the natural and generic method to decompose the single networks into their mesoatomic constituents?

To define mesoatomic elements of TPN morphologies, we propose three basic principles:

(1) The ultimate crystal structure is a symmetric space-filling packing of many copies of a single (or at most, a few) mesoatomic motif(s).

(2) Mesoatom shapes correspond to (average) volumes occupied by specific groupings of molecules (i.e., mesoatom boundaries do not cut across average chain trajectories).

(3) Mesoatoms correspond to thermodynamically/kinetically favored local structures.

(a) Mesoatoms possess high point group symmetry (i.e., the crystal volume includes many copies of a favored subdomain packing motif).

(b) Mesoatom dimensions should be comparable with molecular size.

While the first two propositions guarantee that the ultimate structure could be rebuilt by assembly of the mesoatomic units, the third proposition is motivated by the notion that mesoatoms identified in the final structure can be connected to groups of molecules that are likely to preassemble under many growth conditions. To that end, proposition (3.a) implies that packing adopts multiple copies of a favored local geometry, conferring it with a low free energy, while (3.b) is a requirement for the reasonably fast nucleation time to form (micellelike) aggregates. Of course, (3.a) and (3.b) do not themselves guarantee that such an arrangement is kinetically favored under all conditions without careful consideration of the nonequilibrium pathways of formation, but we nevertheless argue that these principles provide a reasonable zeroth-order framework to extract likely candidates based only on geometry, topology, and symmetries of the final phase morphology and one which can be generalized to self-assembled crystals with more complex domain topologies than spheres and cylinders.

Next, we describe how these physical principles can be translated into a prescription for identifying the mesoatoms from a final TPN crystal of a BCP melt. This approach breaks into three steps:

Step (1): Divide the ultimate crystalline structure into individual domains (i.e., single networks).

Step (2): Identify the centers of the mesoatoms as the set of highest point symmetry positions (i.e., Wyckoff sites) fully enclosed by the single-network domains.

Step (3): Divide the single network into volumes according to the mesoatom centers.

These three steps are illustrated in Fig. 2 for mesoatoms within 1 of the 2 SG domains of the DG.

In this case, the mesoatom centers correspond to Wyckoff positions 16*b*, which are situated at the center of 3-valent junctions (black spheres in step 2 of Fig. 2). These positions are the intersection of 3 twofold rotation axes that meet along a threefold rotation axis normal to the plane spanned by the twofold axes, which run along the struts of the skeletal graph of the (10,3) network. This D_3 point symmetry (or .32 in Hermann-Mauguin notation) implies that there are six copies of the same asymmetric motif in this region. Notice that there are Wyckoff positions (24*c*) that sit at the centers of struts between 16*b* sites, but these have point symmetry (D_2) with fewer (4) copies of fundamental (asymmetric) local packing motif than position 16*b*. (In terms of the number of copies of asymmetric unit per Wyckoff position, it is intuitive that positions with the greatest number of motif copies per site have the highest point symmetry.) As we discuss in more detail below, while Wyckoff position 16*a* (with point symmetry C_{3i}) has the same number of asymmetric motifs (when accounting for point inversion), this position sits at the terminal boundary between two SG domains, and as such, it cannot be used to define the center of a mesoatom. We note that, as consequence of these rules and the particular symmetry of the DG crystal, we find that DG mesoatoms split into two opposite chi-

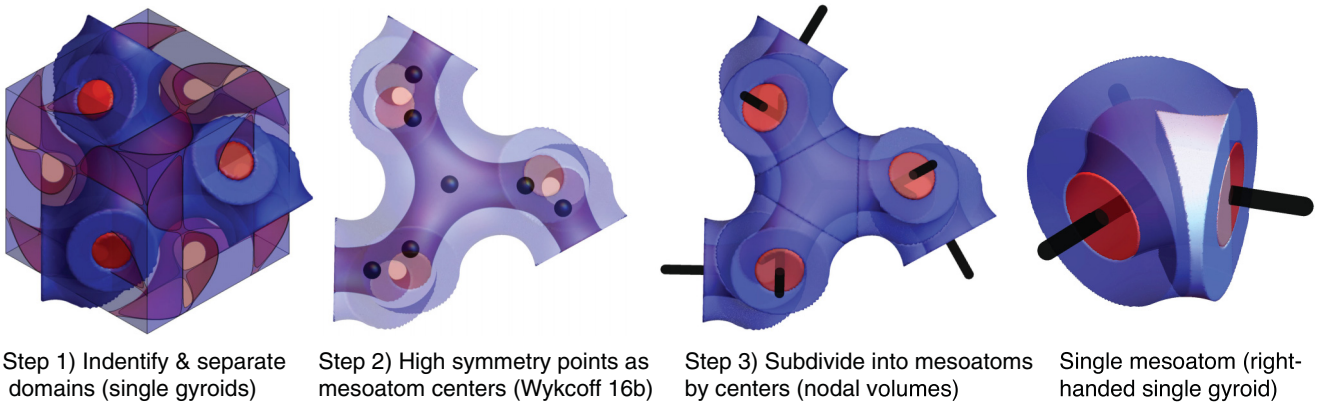

FIG. 2. Mining the mesoatom. Schematic sequence of domain-to-mesoatom decomposition in + network domain of the double gyroid (DG). On the right, we show the final (enlarged) mesoatom, with the black tubes highlighting the portion of the single-gyroid network to which it belongs. Additionally, we highlight that this mesoatom itself is composed of 6 copies on the asymmetric unit (highlighted in lighter colors) that can be generated by the elements of the D_3 point symmetry.

ralities, consistent with their centers at noncentrosymmetric site 16*b*.

In Fig. 2, we show the last step is to divide the gyroid domains according to their centers (at 16*b* sites) into mesoatoms. Strictly speaking, proposition (2) above requires that this dividing surface avoids crossing through mean molecular trajectories (see Discussion in Sec. V.A). Specifying such a surface, of course, requires some detailed knowledge about the mean trajectories of those molecules, such as could be provided via BCP tessellations used in strong-segregation theory calculations [31,35]. However, to a good approximation, chains along the struts between nodes of the DG (or other networks) tend to radiate roughly normally to the so-called skeletal bond that connects between the node centers (a more accurate picture has trajectories extending from 2D weblike terminal surfaces [25]). Hence, for our purposes, we approximate surfaces that divide between neighbor mesoatoms as planes normal to those skeletal bonds (i.e., local chain trajectories are assumed to be parallel to those dividing planes). Partitioning the network into mesoatoms of equal volumes is performed by perpendicularly bisecting the plane through the struts of the SG separating two neighboring 16*b* sites.

The result of this process is shown in Fig. 2, with two sets of mesoatoms required for the DG assembly. Each mesoatom is chiral, deriving from one of the two enantiomeric SG domains, and inherits the D_3 symmetry of the 16*b* sites as well as $\frac{1}{16}$ of the volume of the cubic $Ia\bar{3}d$ unit cell. Notably the nonconvex shapes of these DG mesoatoms (as well as the counterparts for DD and DP) are more complex than the polyhedral mesoatomic shapes expected from simple crystals of spherical domains (e.g., BCC and FCC). The obvious distinction is that mesoatom volumes form DGs, and other TPNs are bounded by two types of surfaces: negatively curved and approximately minimal surface faces and roughly planar faces derived from subdivision of the single-network domains into high point symmetry objects. These two types of surfaces correspond to contact between mesoatoms of two distinct types: internetwork (the saddle faces) and intranetwork (quasiplanar strut faces). In the following sections, we analyze the shapes of these complex mesoatomic particles, their local packing geometry in the DG, as well as their counterparts in DD and DP.

III. ANATOMY AND PACKING OF MESOATOMS: DG, DD, AND DP

We now describe the geometric features of mesoatoms defined by the decomposition principles mentioned above for the three canonical cubic double networks: DG, DD, and DP. For the purposes of modeling the principal shape characteristics, we model the terminal surfaces dividing the two single-network domains using the single-Fourier mode level set approximation to the gyroid, diamond, and primitive TPMSs [36,37]. Given a diblock copolymer domain, and particularly an IMDS for the structure, better approximations to this terminal boundary could be constructed from the medial surface in the matrix domains. Again, we make the assumption that mean chain trajectories are well approximated as normal to the skeletal bond between two nodes (i.e., mesoatom centers), such that the faces that divide two neighbor mesoatoms within the same network are planar and perpendicular to those bonds (struts). We expect these approximations are sufficient to capture the primary structural mesoatomic motifs of distinct structures, although one should also expect at least subtle variations in the detailed shapes of both the internetwork and intranetwork face shapes, not to mention questions about temporal evolutions, thermal fluctuations, and distortions away from any idealized shape, a point that we return to in the Discussion (see Fig. 15).

Figure 3 shows the mesoatomic units for the three cubic double networks, highlighting the topology of distinct networks with black or white struts that protrude through the strut faces according to whether the units belong to the + or − network domains, and a view of mesoatoms whose centers belong with a cubic repeat of the structures (the translational symmetry of DG and DP are body centered, while DD is primitive). Very briefly, the shapes of these mesoatoms are constructed following the three steps defined above, using a (single-Fourier mode) level surface approximation [36,37] for the minimal P, D, and G surfaces (for DP, DD, and DG, respectively) as a model of the matrix terminal boundary that divides the double networks into two continuous domains.

Notably, like the DG mesoatom introduced above, for DD and DP, mesoatoms are centered on the nodal centers of the

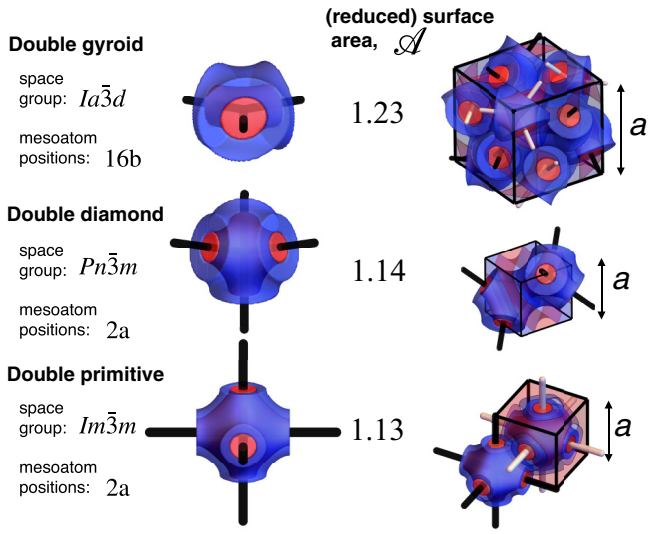

FIG. 3. Comparison of mesoatoms of the cubic double-gyroid (DG), double-diamond (DD), and double-primitive (DP) phases. The right-most column highlights volumes of mesoatoms whose centers lie within an elementary cubic repeat of each crystal. The struts emanating from the faces of the mesoatoms are colored black and white to indicate which of the two networks they belong to (referred to as + or − networks in the text).

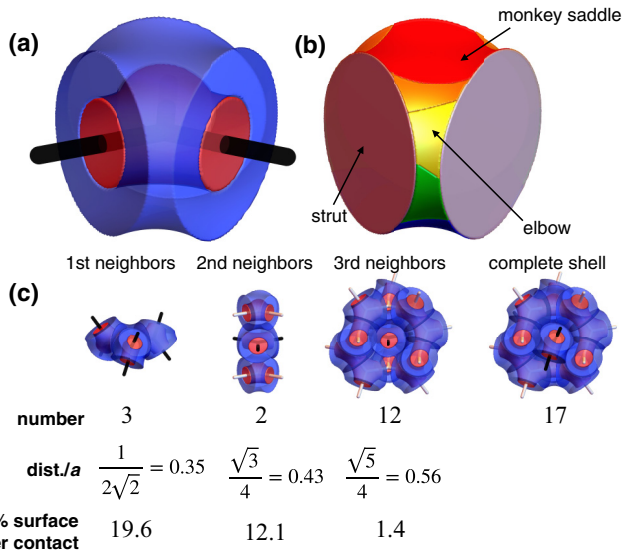

FIG. 4. Shape and packing of double-gyroid (DG) mesoatoms. (a) One of the elementary DG mesoatoms which is recolored in (b) in terms of the regions of contact between the 17 neighboring mesoatoms that touch its surface. These neighbors fall into 3 distinct sets according to their center-to-center distance and surface contact as detailed in (c).

single network, corresponding to sites of tetrahedral or octahedral coordination, respectively. Additionally, mesoatomic shapes are bounded by two types of surfaces: saddled-shaped surfaces that divide between neighbors on different networks and planar faces that divide between neighbors on the same network. We note that the DG structure is composed of two sets of chiral mesoatoms and that chirality is reflected in the shape of the saddle skin, closely following the chiral shape of an oriented gyroid surface [34].

Given the mesoatom shapes extracted from the final morphology, it is straightforward to analyze and compare their basic geometry. As nonconvex volumes, it is intuitive that such shapes are bounded by relatively large surface area. Indeed, the dimensionless surface-to-volume ratio (or equivalently the isoperimetric quotient) is commonly invoked in either heuristic or geometric theory for symmetry selection in crystals of quasispherical mesoatom domains. Here, we measure this by

$$\mathcal{A} \equiv \frac{(\text{area})}{[36\,\pi\,(\text{volume})]^{\frac{2}{3}}},$$

which is the ratio of the bounding surface area (including strut and saddle boundaries) to the area of an equal volume sphere, a dimensionless number that is strictly $\geqslant 1$. For comparison, for the (mostly) convex polyhedral cells for sphere packings, like BCC or even more complex Frank-Kasper variants, $\mathcal{A}$ is the in the range 1.09–1.1 [13,20], in this sense, roughly 10% more area than the spherical volume. The dimensionless area values for mesoatoms of cubic double networks are shown in Fig. 3, indicating increases of the surface area $>\sim$ 5–12% higher than the mesoatomic elements of spherical domain crystals, an intuitive consequence of the nonconvex shapes of network mesoatoms. The hexavalent DP mesoatom with the highest point group symmetry (O_h), whose shape is like a truncated octahedral shape of the BCC Voronoi cell, is lowest among the network mesoatoms. Network meosatoms with the lowest point group symmetry, trihedral DG mesoatoms, exhibit a substantially larger area.

Beyond the basic geometry of individual shapes, the mesoatomic decomposition provides valuable insights into the local packings of contacting-neighbor units, which differ considerably between the network types. We begin by describing local packing of a DG mesoatom and its surrounding first shell of neighbors, corresponding to the set of mesoatoms sharing contact with the surface of a central particle. As shown in Fig. 4, DG mesoatoms have 17 contacting neighbors, which are classified into three sets according to the center-to-center distances. A DG mesoatom has three nearest neighbors, which are strut neighbors belonging to the same SG network (and hence have the same chirality) whose centers belong to the common plane of the 3 twofold axes. The remaining 14 neighbors belong to the other gyroid network and are in contact with the central mesoatom along its saddle surface. In this set, there are two next-nearest neighbors, which are situated above and below the threefold axis of the central particle (i.e., stacked along a ⟨111⟩ direction). These stacked pairs nestle along minimal monkey-saddle-shaped regions. The remaining 12 third-nearest neighbors contact the central particle along the elbow regions of the saddle surface that span between two struts.

In Fig. 4(b), we color the surface of the DG mesoatom according to these regions of local contact, and in Fig. 4(c), we give the fraction of the surface that is contacted by a neighbor of each of these types. In this way, we see that most of the neighbor contact (57.6%) is composed of like-network strut neighbors. The remaining fraction is split between the

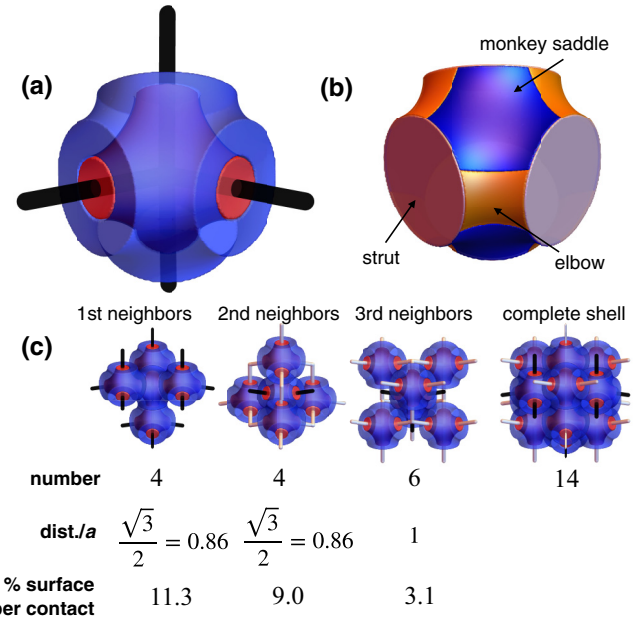

FIG. 5. Shape and packing of double-diamond (DD) mesoatoms. (a) One of the elementary DD mesoatoms which is recolored in (b) in terms of the regions of contact between the 14 neighboring mesoatoms that touch its surface. These neighbors fall into 3 distinct sets according to their center-to-center distance and surface contact as detailed in (c).

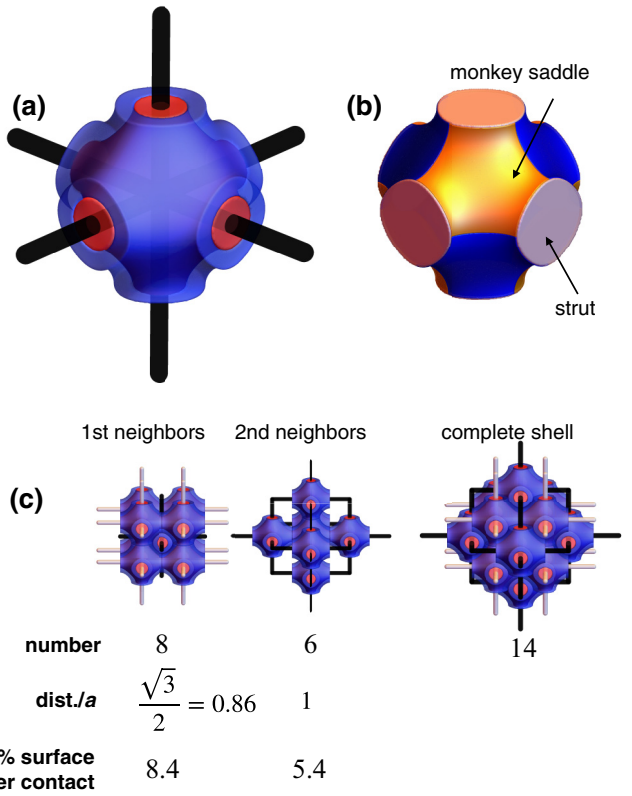

FIG. 6. Shape and packing of double-primitive (DP) mesoatoms. (a) One of the elementary DP mesoatoms which is recolored in (b) in terms of the regions of contact between the 14 neighboring mesoatoms that touch its surface. Center-to-center distance and surface contact of two distinct sets of neighbors detailed in (c).

2 monkey-saddle neighbors (24.2%) and the 12 elbow neighbors (16.8%). Not unlike the better-known case of Voronoi polyhedra, here, we also find that contact area decreases with neighbor separation (center to center). Due to the very unequal distributions of contact areas between the two populations, intranetwork contacts dominate the surface coverage of DG mesoatoms, even though they are overwhelmed in number 14:3 by internetwork contacts. Below, we consider the potential ramifications of the contact area distributions between neighbors for physical models of mesoatom association during crystal formation.

Figures 5 and 6 show the corresponding analysis of the local mesoatom packing for DD and DP, respectively. Relative to the DG mesoatoms, these structures exhibit a few key differences. First, the mesoatomic units of DD and DP are achiral and hence equivalent (up to rotations) between the two single-network domains. Second, they exhibit a smaller fraction (less than half) of their contact with intranetwork (a.k.a. strut neighbors): 45% for DD and 32% for DP. The DD packing is still like DG in that its closest (and highest contact) neighbors belong to the same network, with its second- and third-nearest neighbors belonging to the second diamond network domain. However, DP packing has a distinct pattern where its closest highest-contact neighbors are its 8 monkey-saddle faces with the second primitive network domain, while its 6 lower-contact strut neighbors are more distant yet belong to the same primitive network domain.

Taken as sequence, the mesoatomic shapes from DG to DD to DP represent a progressive increase in the number of point symmetry elements (and asymmetric motif copies) from 6 to 24 to 48, respectively, in addition to the corresponding increase in network valence. Along with this increasing symmetry, we observe a transition in the distribution of intranetwork and internetwork neighbors in the constitutive mesoatomic units of the double networks. In lower-symmetry/coordination structures, like-network mesoatoms are relatively closer and have higher contact, sheathed by a larger number of more distant neighbors of the opposing network. While in higher-symmetry/coordination structures, internetwork saddle contacts are pulled closer and strut contacts are pushed out, lowering the intranetwork contact per mesoatom. Notably, for the highest symmetry DP mesoatoms, a distinct set of elbow contacts are absent, with the entire saddle surface taken up by a single set of monkey-saddle contacts.

Lastly, we note that the distinct neighbor correlations of mesoatoms also encode the local topology of the network assemblies, shown in Fig. 7. For each of the cubic double networks, the internetwork neighbors in the first complete shell of neighbors (i.e., the contacting mesoatoms) compose the f elementary loops that catenate the f struts emerging from a central mesoatom (i.e., each of the struts emerging from a node is looped by neighbors in the contacting shell of mesoatomic neighbors). For DG, loops are composed of two series of 4 elbow neighbors that join at the 2 monkey-saddle neighbors that sandwich the central mesoatom (i.e., loops of 10 total). As a set, the 14 internetwork mesoatoms form a

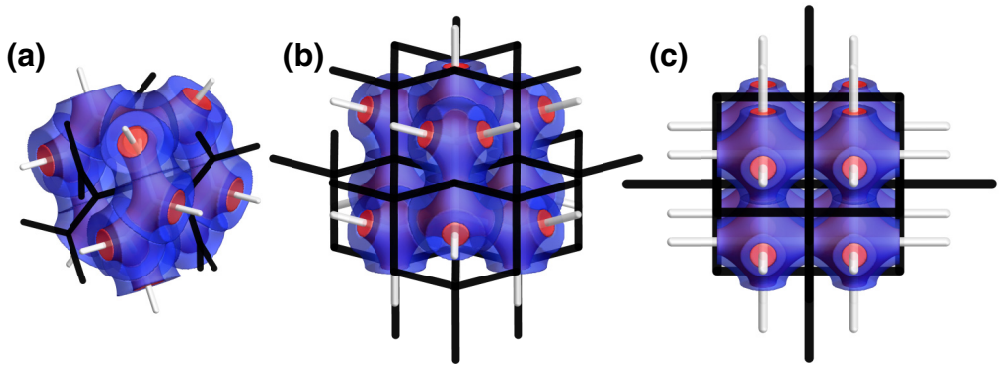

FIG. 7. The set of catenating mesoatom neighbors on the − (network) that envelope a central mesoatom on the + network (black) are shown for the (a) double-gyroid (DG), (b) double-diamond (DD), and (c) double-primitive (DP) phases. The (black) skeletal bonds of the catenated+connected to the central mesoatom are shown to illustrate the local bond topology.

trihedral cage that enmeshes the central particle and encircles each of the like-network struts that emerge from it. Similarly, the 10 and 8 internetwork mesoatoms for DD and DP, respectively, compose tetrahedral and cubic cages for these networks [38].

In the following section, we consider how the local geometry neighbor contact encoded in the shapes of mesoatoms plausibly templates the kinetics of intercatenation in a simplistic model of assembly.

IV. MESOATOMIC IMPLICATIONS FOR NETWORK CRYSTAL FORMATION: A MINIMAL MODEL

In the prior section, we described the elementary mesoatomic molecular groups of tubular network crystals extracted using symmetry-based principles from the final equilibrium morphologies of neat diblock copolymer melts. In this sense, these shapes describe the mature state of these mesoatomic elements, as opposed to transient structures occurring as the system evolves toward the idealized equilibrium state. Here, we proceed one step further to consider how the anisotropic shapes of these mesoatomic elements might provide a plausible basis to template the nonequilibrium kinetic pathways to long-range-ordered and topologically nontrivial double-network crystals. Noting that these so-defined mesoatoms pack perfectly to tile space and moreover possess outer terminal surface shapes that would likely promote and stabilize strong orientational correlations between neighbors based on shape complementarity alone, we ask the basic question: How would particles with the shapes of such mesoatoms assemble? In the context of BCP melt assembly, this model proposed assumes that, under relevant conditions, mesoatomic groupings of molecules form first, and to a good approximation, the shapes and packings of the ultimate mature mesoatoms then template the kinetics of higher-order crystal formation. Assuming preformed mesoatoms, we consider the simplest possible assembly model for the local interactions between those mesoatomic units and, from this, model the nonequilibrium process of crystal growth and intercatenation between constituent network domains. We leave the numerous open questions raised by this proposition (e.g., how might more realistic models incorporate dynamic evolution or cooperative distortion of mesoatoms into the assembly process?) for a later discussion.

Schematically, the underlying assumptions of this minima model are summarized in Fig. 8. Crudely, the process is split into two parts. First, we assume that assembly kinetics favors rapid preassembly of primordial mesoatomic groups. Second, these primordial mesoatoms assemble into multimesoatom crystalline structures, with the relative affinity for mesoatom addition predicted by the contact geometry of the ultimate mesoatomic shapes. Implicitly, the model assumes that the mesoatoms take their ultimate highly nonconvex shapes by the time they bind to the face of an existing multimesoatomic cluster. We emphasize that the initial shape of the priomordial mesoatom may be variable, ranging from spherically symmetric micellelike shapes to potentially lower-symmetry shapes that may be intermediate in shape to spheres and the ultimate mature mesoatom shape. In the former case, it would be necessary that the mesoatom is reshaped upon binding, while in the latter, it is possible that some of the nonconvex shaping may take place in the priomordal state. This latter case would be the case when the local shape energetics of molecular packing internal to the mesoatom strongly favors a local saddle-wedge geometry over, say, spherical or cylindrical conical wedges, as can be predicted from models that vary the shape motif of local packing [35,39]. Notably, while specific rates between these extreme scenarios may depend significantly on whether malleable mesoatoms assume their forms preassembly or else get into shape upon binding, the basic predictions of our model will be unchanged since our underlying assumption is only that the mesoatomic groups add to an existing cluster in the most energetically favorable location, as we now describe in detail.

A. Model

Our model considers simple nonequilibrium growth kinetics of TPN crystals via the sequential binding of nodal particles whose shapes and contact geometries are determined by the mesoatomic shapes described in Figs. 5–7. We consider a process driven by a simplistic model of mesoatom interactions in which the binding energy of cohesive interactions between mesoatoms is purely determined by their mutual surface area of contact. We consider in turn each of the DG,

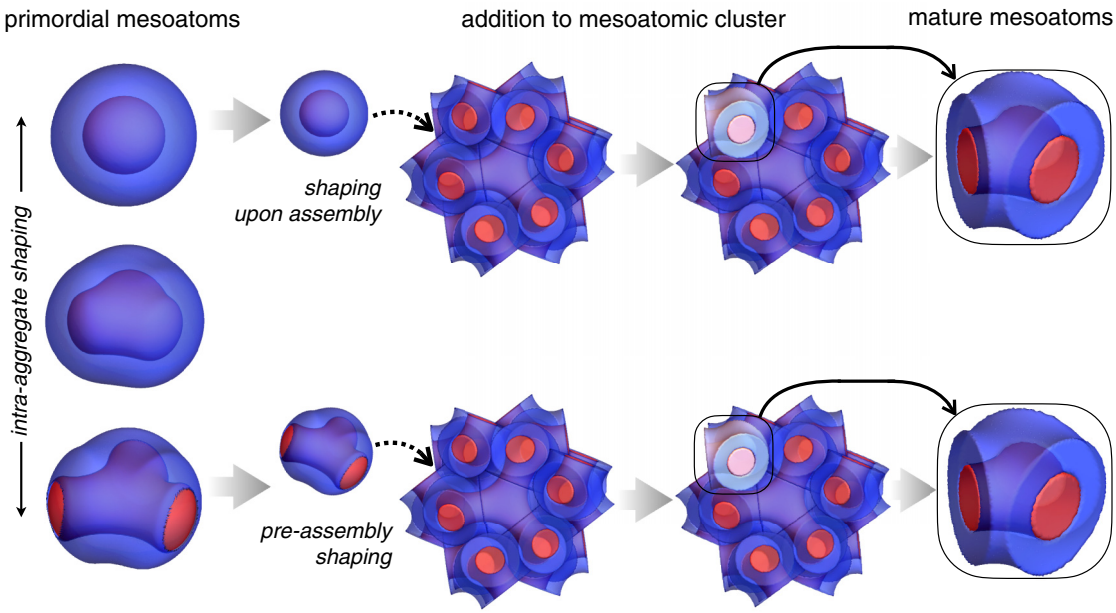

FIG. 8. Schematic illustration of the range of assembly kinetics which underly the considerations of the minimal mesoatomic assembly model, with the left column showing a range of possible primordial mesoatomic shapes which form first prior to assembly into multimesoatomic crystals. The top row highlights a pathway in which spherically symmetric mesoatoms adopt their nonconvex shapes only upon addition to growing crystal, while the bottom row highlights a pathway in which intramesoatomic packing leads to partial evolution toward the ultimate mature mesoatom shape prior to assembly. Our model assumes, for both extremes, that mesoatoms add to the most energetically favorable location in a growing crystal.

DD, and DP structures: the DG with its 3 strut bonds and 10 mesoatoms per loop, the DD with its 4 strut bonds and 6 mesoatoms per loop, and the DP with its 6 strut bonds and 4 mesoatoms per loop.

Defining ϕ_{ij} as the fractional surface contact between neighbor mesoatoms i and j (i.e., $\phi_{ij} = 0.196$, 0.121, and 0.014 for first, second, and third neighbors of DG mesoatoms), the energy of a cluster of mesoatoms is

$$E \equiv -\sum_{\langle ij \rangle} \phi_{ij},$$

where the sum is taken over occupied neighbor pairs of mesoatoms. Implicitly, this model neglects possible differences in the (free) energies of contact between strut neighbors (like-network) and saddle neighbors (internetwork), which could arise due to entropic differences of brush domains meeting parallel to or perpendicular to mean chain directions. Also, surface energy of different faces may vary due to enthalpic differences in the cohesive free energy density in tubular and matrix blocks and the composition differences at those faces, which, e.g., would depend on the relative solvent quality and concentration for solution-cast assembly. For ordered phase formation from a higher-temperature bulk melt state [via the order-disorder transition temperature (ODT)], there is obviously no effect of solvent on cohesive free energy density nor variation of the volume fraction of the subdomains via a preferential solvent. Neglecting these potential physical chemical factors implies that the differences in mesoatomic binding energies derive purely from the complementarity of their anisotropic shapes. In addition, we assume that rigid mesoatomic units only bind in perfectly oriented and spaced arrangements (i.e., their centers can only lie on the appropriate set of Wyckoff positions and adopt orientations consistent with the symmetry required by the space group of the ultimate crystal structure). Such a model considers mesoatom surface interactions to be extremely short range and further assumes that the complementarity of the nonconvex shapes restricts relative rotations. The latter effect is quite plausible for nested contacts between the threefold monkey-saddle faces, which provides a mechanism to template the long-range order and complex topologies of double-network crystals even at the level of two-body contacts.

Assembly is modeled as a kinetic process following very simple nonequilibrium dynamics, which adds the $N+1$ mesoatom to an existing cluster of N mesoatoms at the available location with the lowest total binding energy. Hence, after each step of the assembly process, the unoccupied neighbor positions of all N particles are scored according to the total binding energy of adding the mesoatom at that position, and the next mesoatom is added to the boundary position with the strongest binding. If there are multiple locations with the same minimal binding energy, one of those degenerate sites is simply chosen for mesoatom placement. In this way, assembly is modeled via a greedy kinetic pathway that lowers the energy by the largest possible amount at each step, following a process that is irreversible and largely deterministic (except for degeneracy of the strongest binding positions). While there obviously is no guarantee that the state clusters are close to ground states, this simple algorithm allows us to explore the interplay between local packing, mesatomic binding, and topological evolution via a plausible dynamic scenario for crystal growth. It is, of course, possible to consider more complex sampling approaches, for example, which attempt to

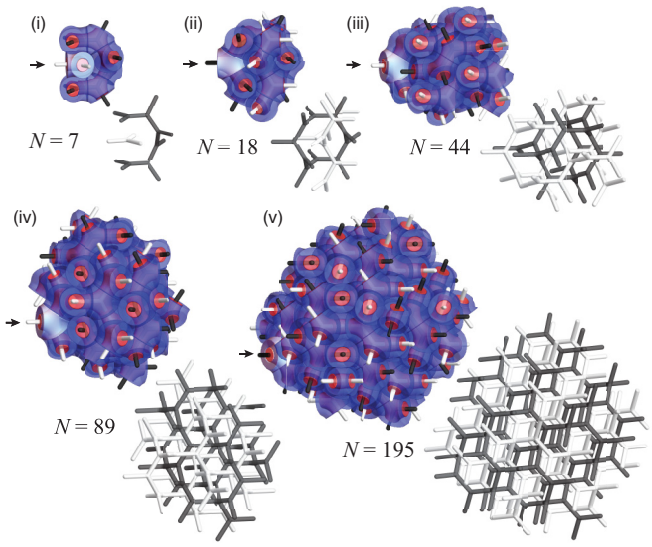

FIG. 9. Snapshots of the simulated growth of double-gyroid (DG) crystals for distinct numbers of added mesoatoms N. For each, the most recently added Nth mesoatom is highlighted by coloring the outer terminal surface of that mesoatom white. The skeletal bonds for occupied mesoatom positions are shown from the same viewing direction with the mesoatom volumes removed.

consider near-equilibrium assembly conditions at controlled chemical potential and temperature.

Below, we first discuss the results of this simple model for growth of DG crystals, focusing on the evolving topology of double-network assembly. We follow this with a comparison with the growth of DD and DP crystals and finally briefly discuss results of the model for facet formation for growing crystals.

B. Results—DG assembly

We begin with the case of DG crystal assembly. Here, we note the kinetic growth algorithm considers addition of DG mesoatoms without explicit bias for chirality (i.e., both DG mesoatomic enantiomers maintain fixed, equal availability). Figure 9 shows several snapshots of the growth of a crystalline DG cluster up to $N = 195$ mesoatoms, showing both the space-filling structure of assembled mesoatoms as well as the skeletal bonds corresponding to those assembled mesoatoms. In each of those snapshots, the final (Nth) mesoatom added to the cluster is highlighted with a white shading of its outer terminal surface. In Movie 1 in the Supplemental Material [40], we show an animation of the sequence of mesoatomic additions for a cluster growing up to $N = 89$ units.

To understand how the local packing of DG elements templates the dynamic intercatenation of the double-network crystal, we analyze the coevolution of binding energetic and network topology with increasing cluster size. In Fig. 10, we plot the binding energy per subunit $E(N)/N$ as well as $\Delta E(N) = E(N) - E(N-1)$, the binding energy of the Nth mesoatom, with points colored black/gray according to whether the Nth mesoatom joins the +/− SG network, respectively.

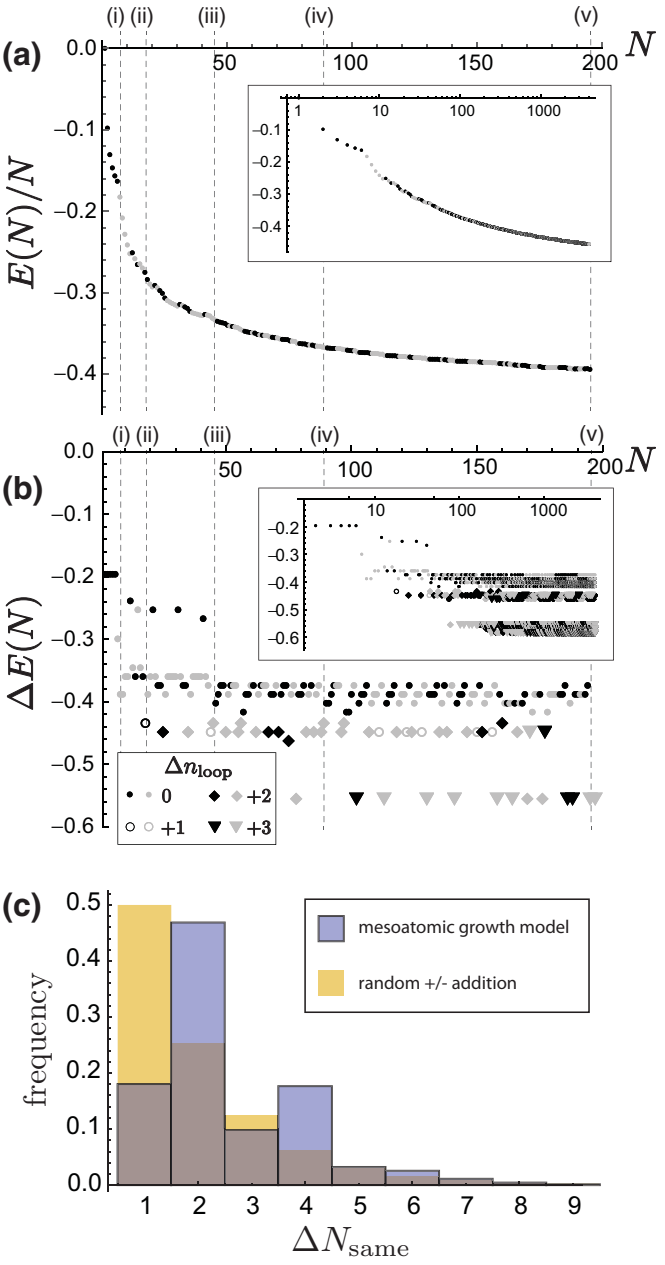

FIG. 10. (a) Plots of the binding energy density of simulated double-gyroid (DG) crystals vs mesoatom number, with each point colored according to + (black) or − (gray) network placement of the Nth mesoatom. (b) Plots the binding energy of the Nth particle vs N and indicates the number of closed loops added upon binding. The dashed lines indicate snapshots (i)–(v) shown in Fig. 9. (c) Plots the frequency of consecutive mesoatom additions to the same networks of length, ΔN_{same}, with mesoatomic simulations shown in blue and random (uncorrelated) additions shown in orange for comparison.

First, we observe a notable alternation for mesoatom addition between the networks, in which sequences of a few mesoatoms add to the same network before switching to the opposing network. The basic origin of this effect is easiest to understand for the first sequence of 7 mesoatoms [up to the first snapshot in Fig. 9(i)]. Because strut-strut face bonds are most favorable among all contacts, the first neighbor in the

cluster is added as the closest neighbor in the same network. Such strut bonds within the same network remain preferred for the next several steps up to the $N = 6$ mesoatom because the total amount of saddle surface contacts a possible neighbor on the alternate network results in weaker binding than $\Delta E_{\text{strut}} = -0.196$. This situation persists until the cluster forms $\frac{6}{10}$ths of a closed loop of a single network. Such a structure is formed by black network mesoatoms in Fig. 9(i). For this configuration, it is straightforward to see that the partial loop envelops a high binding energy pocket, wherein a single additional particle (on the opposite network) can simultaneously form 2 monkey-saddle bonds plus 4 elbow bonds, resulting in a binding energy $-0.298 > \Delta E_{\text{strut}}$ which is stronger than an additional intranetwork strut bond. Hence, before closing the first loop, the assembly switches to the alternate network and proceeds to add to that network the next sequence of 5 mesoatoms. From this point, the mesoatom addition alternates back and forth, as partially completed network loops create new strong-binding pockets via their saddle faces.

Given this alternation of added particles between the networks, the formation of the first loop in the structure does not occur until the 18th mesoatom is added [snapshot of Fig. 9(ii)], far more than the minimum 10 mesoatoms needed to form a single loop of the gyroid network. In Fig. 10(b), the binding events are labeled according to the number of network loops (0, +1, +2, or +3) added. Added loops are labeled as open circles (here, *loops* are counted as the filled 10-mesoatom fundamental cycle of the gyroid graph), showing clearly that these binding steps are particularly strong binding events due to the addition of at least 2 intranetwork strut bonds, generically exhibiting lower energies than binding events that leave the topology unchanged. This suggests that cluster states that correspond to loop closure in the Nth mesoatom addition will be particularly stable and relatively longer-lived states of growing DG crystals.

In the sequence of the first 4000 mesoatom additions, 61% of the binding events leave the number of closed loops unchanged, with the remaining fraction of corresponding binding events increasing the number of loops by +1 (3%), +2 (11%), or +3 (25%). We note from Fig. 10(b) that the most energetically favorable binding events tend to add multiple loops (i.e., +2 and +3), consistent with the addition of a DG mesoatom along a ⟨111⟩ neighbor, creating at least 2 strut (intranetwork) and 1 monkey-saddle (internetwork) bonds, hence resulting in a large binding energy $= -0.513$.

We next analyze the alternating network growth kinetics in the model of DG growth in terms of the number of sequenced mesoatoms that add to the same network (ΔN_{same}). In Fig. 10(c), we plot the frequency of ΔN_{same} like-network additions for clusters up to $N = 4000$. For comparison, we also plot the (exponential) distribution that would be expected if the subsequent binding to + or − networks was completely uncorrelated. This shows the relative excess of 2- and 4-mesoatom runs to the same network. While this is indicative that strong intranetwork binding promotes like-network correlations, $\langle \Delta N_{\text{same}} \rangle = 2.6$, which is much less than the length of the 10-atom loop, consistent with the observation that additions switch back and forth multiple times between loop closure events in the DG crystals.

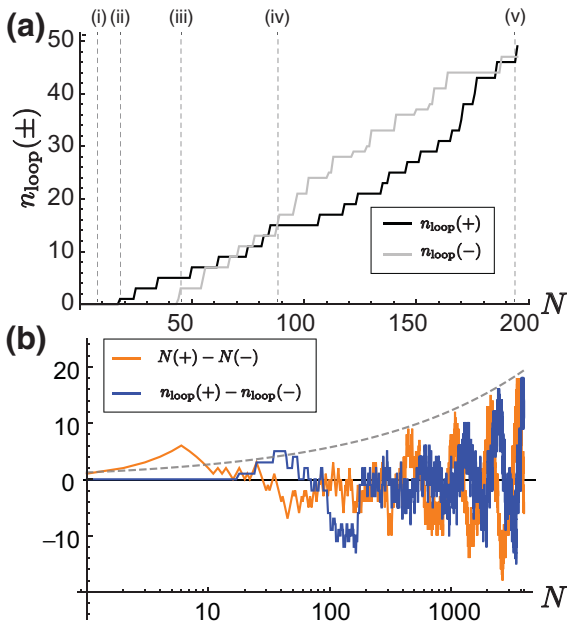

FIG. 11. (a) Plots of the number of closed loops in the + and − networks in the simulated double-gyroid (DG) crystal vs mesoatom number. (b) Plots the +/− excess of mesoatom number and loop number vs number of added mesoatoms in the DG crystal. The dashed line has the scaling $N^{1/3}$, discussed in the text.

In Fig. 11, we plot the kinetics of loop formation in the growing DG cluster. We first focus, in Fig. 11(a), on the number of loops $n_{\text{loop}}(\pm)$ in the 2 SGs (denoted as + or −) in the early stages of cluster growth illustrated in the highlighted snapshots of Fig. 9. Beyond the latency of the first loop forming after the 18th particle, we observe a surprising asynchrony in the looping of the two networks. The first three loops form in the same + network, well before the opposing − network forms even its first loop at the $N = 44$ mesoatom [shown in the snapshot in Fig. 9(iii)]. Following this, a rapid sequence of 2 loop additions in the − network quickly equalizes with the + network, eventually overtaking looping in that network after the $N = 89$ mesoatom [shown in the snapshot in Fig. 9(iv)]. The cluster maintains an excess of − loops over a fairly large span, up to the $N = 195$ mesoatom [shown in the snapshot in Fig. 9(v)], after which point the looping in networks remains fairly equal from several additional mesoatoms.

In Fig. 11(b), we plot the differences in the looping between the two networks, as well as the difference between the total number of mesoatoms in each network, for cluster growth up to $N = 4000$. This shows that the initial loop imbalance roughly equalizes between $N = 195$ and $N \sim 1000$ but at longer times starts to exhibit a more regular sawtooth pattern alternating swings of + or − loop excess. For $N > 1000$, loop excesses seem to be in lockstep with broader swings in the excess numbers of mesoatoms added to + vs − networks albeit with a lag between loops and mesoatom excess. This, in combination with the fact that their magnitude grows with N, seems to suggest these fluctuations are dictated by fairly regular patterns of surface layer growth, presumably with steps of the surface growth exposing different numbers of strong binding pockets on the like vs unlike gyroid networks

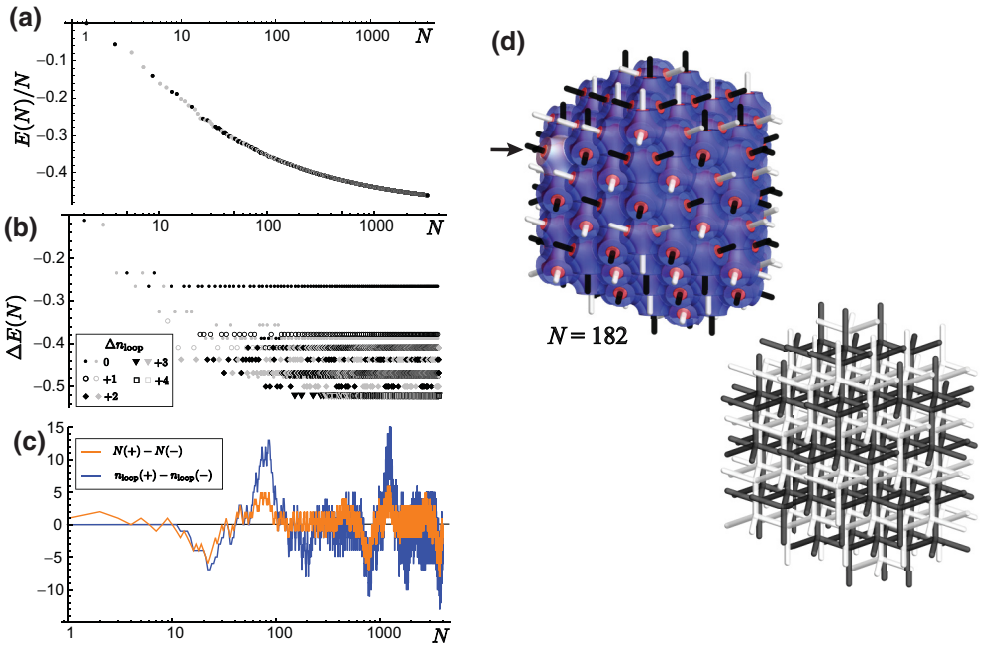

FIG. 12. Results of simulated mesoatomic growth double-diamond (DD) crystals, showing (a) energy density, (b) binding energy, (c) +/− network excess vs number of added mesoatoms for up to $N = 4000$. (d) shows a snapshot of a growing cluster of simulated DD mesoatoms and the skeletal network of bonds corresponding to occupied mesoatom positions.

along distinct regions (i.e., facets) of the growing crystal. We return to the geometry of growing facets in the crystal below.

C. DD and DP assembly

The above results for the mesoatomic model DG assembly illustrate how the local shape and packing of the nonconvex building blocks of double-network crystals template the dynamics of intercatenation. Here, we compare results for our deterministic model of mesoatomic crystal growth for the higher coordination DD and DP networks.

As shown, in Figs. 12(a) and 12(b), compared with predictions for DG [Figs. 10(a) and 10(b)], addition of mesoatoms in DD alternate much more frequently between the disjoint networks, even at the early stages. For example, only the first 2 mesoatoms bind to the same network before switching to the lower energy binding on the opposite network for the third and fourth particles. This higher alternation reflects the fact that, in comparison with DG, next-nearest-neighbor (internetwork) contacts are closer in surface area to nearest-neighbor (intranetwork) contacts for DD. The higher alternation is also consistent with the smaller loop size: 6 for DD compared with 10 for DG. Distinct from DG, as highlighted in Fig. 12(b), DD assembly exhibits binding events that add up to +4 loops. Compared with simulated DG assembly, such events are likely enabled by the higher coordination (4) of the DD network. Indeed, the lowest energy binding events are triple- or quadruple-looping events [such as the $N = 182$ particle addition highlighted in Fig. 12(d)], corresponding to addition along a threefold ⟨111⟩ direction, forming 3 intranetwork bonds, 1 monkey-saddle internetwork (second nearest neighbor), and 3 elbow internetwork bonds (third nearest neighbor). Within the first 4000 mesoatoms added, 35% binding events do not increase the number of loops with the remaining fraction adding +1 (5%), +2 (40%), +3 (7%), or +4 (13%) network loops. In Fig. 12(c), we observe again the fluctuations in the addition to the two distinct networks of DD. This assembly also shows an initial period of + vs − addition (and looping) imbalance at early stages that recovers to a balanced crystal around $N \sim 100$ mesoatoms. However, unlike DG assembly, in DD crystals, fluctuations of network excess do not seem to show a coherent alternation, at least up to $N = 4000$. Also, there is no significant lag between fluctuations of mesoatom addition to networks and the loop addition, with the latter tending to be simply proportional to the number excess of + vs − mesoatoms in the crystal.

Turning now to mesoatom assembly in the 6 strut-bond DP (results summarized in Fig. 13), whose mesoatoms possess the highest valence and smallest basic loop among the DG, DD, and DP set and who have stronger internetwork bonds than intranetwork bonds, we find several notable distinctions. First, the rate of alternation between network additions between + and − networks is the highest among the 3 cubic network crystals. The mean span of like-network additions in simulated assembly for N up to 4000 $\langle \Delta N_{\text{same}} \rangle$ for DP is only 1.15 compared with 1.7 for DD and 2.6 for DG. The enhanced tendency of DP to rapidly switch between + and − network additions (i.e., 85% of like-network spans in DP assembly include only a single mesoatom) is clearly a result of the stronger binding to internetwork (monkey saddle) faces than for intranetwork (strut) faces in DP relative to the other networks. Second, as shown in Fig. 13(b), DP assembly is characterized by a surprisingly limited distribution of loop additions upon binding. For N up to 4000, 97% of added mesotoms increase the number of loops in structure, and these

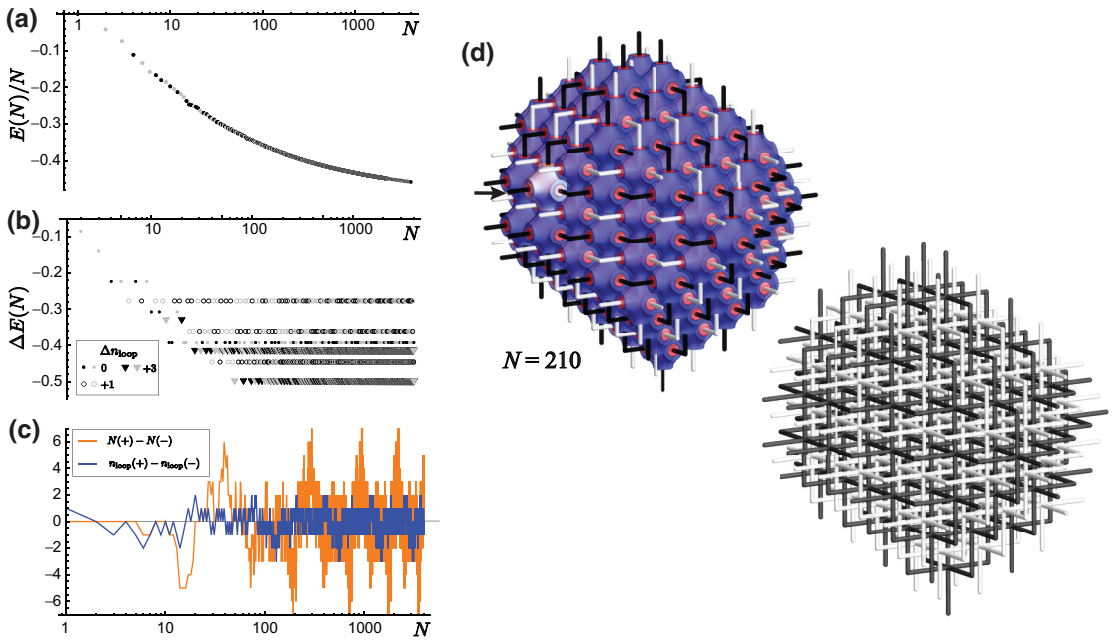

FIG. 13. Results of simulated mesoatomic growth double-primitive (DP) crystals, showing (a) energy density, (b) binding energy, and (c) +/− network excess vs number of added mesoatoms for up to $N = 4000$. (d) shows a snapshot of a growing cluster of simulated DP mesoatoms and the skeletal network of bonds corresponding to occupied mesoatom positions.

are confined to only +1 (24%) and +3 (73%) loop additions. The especially loopy assembly is consistent with the fact that, in the final DP crystal, the ratio of loops to mesoatoms is 3:1, which is a much higher density of loops relative to DD (2:1) and DG (3:2). Last, we observe that, like the DG assembly, the fluctuations in mesoatom and loop addition to + vs − networks in DP crystals [Fig. 13(c)] falls into a regular alternating sequence after an early period ($N \gtrsim 100$), which we again attribute to a repeating pattern of surface growth with successive layers of crystal growth. However, unlike DG assembly [in Fig. 11(b)], the magnitude of these excess fluctuations does not appear to grow with N, suggesting that the network excess is associated with features of the crystal surface that do not grow with size (i.e., vertices of a faceted shape). In the following section, we return to this observation in the context of the emergent external shapes (crystal habits) of single crystals during simulation of double-network crystal growth.

D. Crystal habits

Beyond a detailed picture for evolution of topology in intercatenated network crystals, the mesoatomic assembly model provides direct predictions of the external shape of growing crystals. Equilibrium crystal habits are generically described through the Wulff shapes, which derive from the anisotropic surface energies of distinct crystal facets. The local contact model described above is sufficient to fully determine the surface energetics of DG, DD, and DP crystals (i.e., the distinct surface energies among various Miller planes). Again, while our deterministic kinetics are not guaranteed to sample ground-state clusters for a given N, the model obviously favors growth on high surface energy faces (i.e., particular strong binding directions). Indeed, for sufficiently large clusters, we observe the clear formation of well-defined and stable faceting.

In Fig. 14(a), we show the external surfaces of an evolving DG cluster (viewed from the ⟨111⟩ direction), with the protruding skeletal networks. The sequence shows that, for relatively small clusters (e.g., $N = 125$ and 250), the cluster boundary appears roughly spheroidal, but by $N = 500$ and beyond, the surface shape of the DG begins to exhibit a characteristic pattern, ultimately growing into a cuboidal shape with rounded corners and edges for $N = 1000$. Subsequent snapshots of the surface shape show fluctuations around this basic shape but with the same dominant {100} faces showing apparently the same characteristic fraction of the surface area at late stages.

Similar faceting behavior is found for DD and DP crystals but with large clusters exhibiting different crystal habits. Figure 14(b) shows the $N = 1500$ snapshots for DG, DD, and DP (all viewed from a common ⟨111⟩ direction), with Miller indices of the largest area facets labeled. Notably, the largest faces of the DG crystal are the {100} planes, while in DD and DP, the facet planes are {110} (with minor facets along {211} for DD and DP), yielding habits roughly corresponding to rhombic dodecahedra.

Focusing on the crystal habits of the DG, in addition to {100}-type facets, we also observe prominent {111} facets, leading to a somewhat rounded-cube shape. As well, there are smaller {110} regions along the edges. We note that these {110} facets have normals that correspond to directions of intranetwork bonds, which have relatively strong binding energy compared with the internetwork monkey-saddle bonds along ⟨111⟩, and hence might be expected to possess relatively high surface energies and low facet areas in the corresponding Wulff shape. Notably, the bonds that protrude through the {110} edges for the cuboidal shapes appear to be dominantly

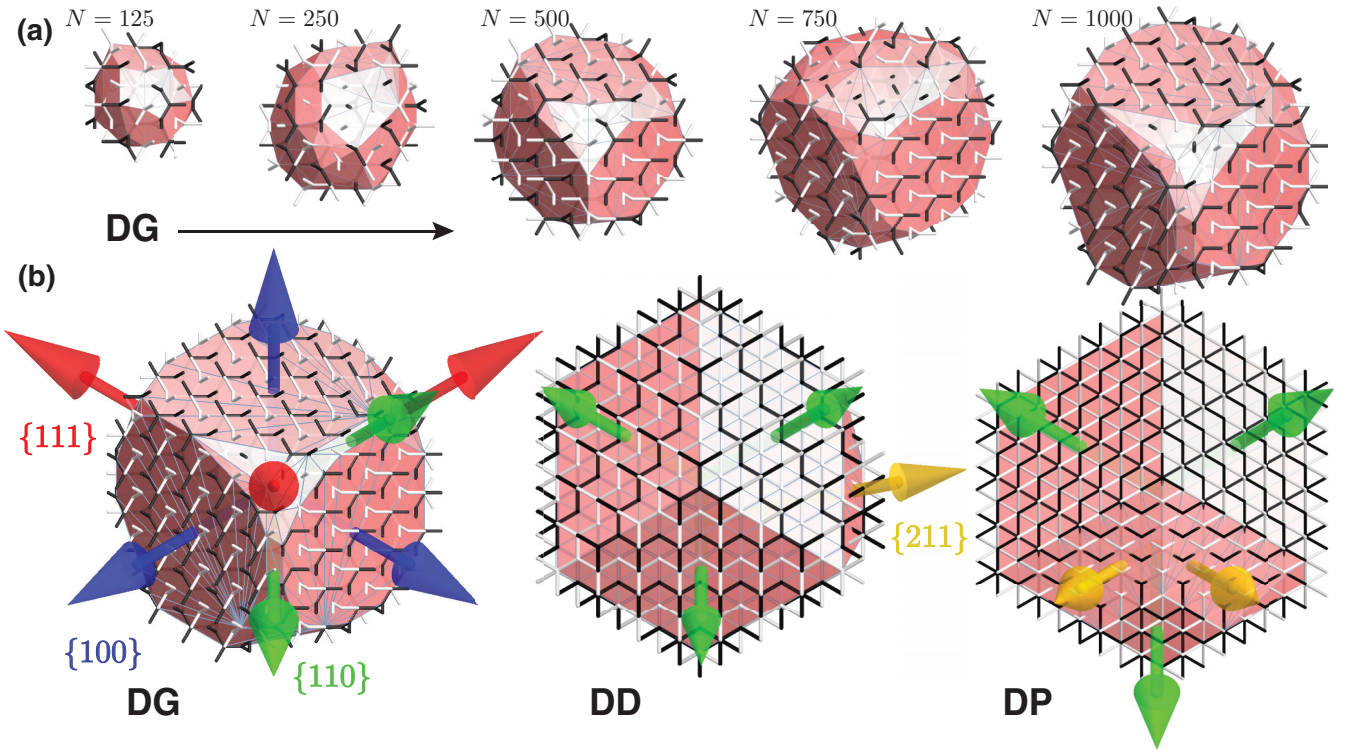

FIG. 14. (a) Growing clusters of double-gyroid (DG) crystals, with semitransparent pink surface facets surrounding the centers of occupied mesoatom positions. (b) shows the crystal habits of simulated DG (left) double-diamond (DD; middle), and double-primitive (DP; right) phases at the $N = 1500$ snapshot, all viewed from a common $\langle 111 \rangle$ direction. The colored arrows highlight the orientation of prominent surface directions on the apparently faceted shapes of the crystals. The apparent breaking of the cubic symmetry in the distribution of facets is a result of the nonequilibrium growth pathways from which the snapshots are taken.

of one network chirality [i.e., in the case shown in Fig. 14(b)]. Thus, if the + vs − excess derives predominantly from these edge regions of the cuboidal crystals, we would expect the fluctuating chiral excess to grow with the edge length as $N^{1/3}$. This scaling is consistent with increasing magnitudes of mesatom excess for DG assembly in Fig. 11(b) (dashed line). This suggests that directional energetics of mesoatom binding could give rise to spontaneous fluctuations of surface chirality (i.e., + vs − excess) that grow arbitrarily large with crystal size. In contrast with the growing asymmetry of DG crystals with N, the + vs − network excess of DP appears to be constant with N, suggesting that this excess is associated with the vertices of the quasipolyhedral crystal (for rhombic dodecahedra, these correspond to the eight $\langle 111 \rangle$ and six $\langle 100 \rangle$ directions).

V. DISCUSSION

A generic construction of the elementary mesoatomic units of supramolecular network crystals, focusing on the cubic double networks of diblock copolymer melts was proposed with the DG as an illustrative detailed example. This generalizes the notion of micellar groupings of molecules that constitute building blocks of three-dimensional (3D) crystalline or 2D columnar arrays of spherelike and cylinderlike domains, respectively, which are ultimately confined to quasipolyhedral volumes that tile the given crystal. Like those cases, mesoatoms of network crystals are associated with maximal-symmetry subvolumes of domains within the equilibrium network crystal (i.e., the set of Wyckoff positions within single domains with the highest point symmetry). Unlike spherical or cylindrical domains, however, mesoatoms in double-network crystals are nonconvex shapes and derive from two types of faces that divide nearest neighbors: planar faces separating like-network neighbors and saddle-shaped faces separating adjacent neighbors on the opposing network.

The mesoatomic construction of network crystals provides a useful structural description of supramolecular network crystals, breaking their complex structure into local motifs, akin to more familiar cellular (e.g., Voronoi) constructions for compact domains. Going beyond this purely descriptive notion, we conjecture that this symmetry- and geometry-based deconstruction provides physical insight into collective properties of network crystals and plausible kinetic pathways by which they form. The three various intercatenated tubular network structures ultimately stem from constraints of packing nonconvex mesoatomic shapes as well as expected differences in physical contact between domains along distinct faces, e.g., saddle faces sit at contact between opposing (matrix) domains, whereas strut faces include contact between both minor and matrix components. The latter distinction suggests an analogy between mesoatomic and atomic crystals in which we view faces that divide brushes on opposing network domains as analogs of noncovalent (i.e., van der Waals) binding, while we associate faces composed of contact between multiple components (strut-bond faces) as analogs of covalent binding. In

this analogy, the total cohesive energy between mesoatoms in double-network crystals includes both covalent and noncovalent contributions, whereas in crystals of spherelike domains, where shapes are polyhedral relatives of Voronoi cells, intermesoatom binding is purely of the noncovalent type.

A. Minimal model of mesoatomic growth: Assumptions and extensions

In the simplest version of the model introduced in Sec. IV, we considered the distinct physical effects of various types of contacting faces to derive the assembled structure purely from the amount and type of same-block–to–same-block surface area of contact, implicitly assuming that free energy of surface contact is independent of which components are in contact and how chains are oriented across the contact faces. It is straightforward to consider generalizations of this simple binding model that relax this constraint. For example, considering the growth of double-network crystals in a solvent that is selective for one or the other component, it is possible to consider how the relative strength of binding along distinct faces would change depending on both the area fractions of minority and matrix components along each mesoatom face as well as the relative surface energetics of solvent contact to those components. For the situation where mesoatoms are forming and then assembling into crystals in a solvent that is selective for the matrix, there would be a correspondingly higher binding along strut bonds, as these better shield the minority domains from solvent contact. This in turn would impact predictions for binding and catenation dynamics as well as for the facet formation in large-scale crystal structures. Stronger (weaker) intranetworks, as should be expected for a solvent selective for the matrix (tubular minority), might be expected to increase (decrease) persistent addition of mesoatoms to the same network ΔN_{same}, thereby alterating the lag dynamics of intercatenation. Alternatively, it may be possible to consider this mesoatomic model for a case where mesoatoms form in a melt, in which case a population of disordered molten chains would serve as the solvent medium in which mesoatoms form and then sample optimal binding on the faces of a growing double-network crystal. In this context, the mesoatomic model provides a natural and predictive framework to understand how highly interconnected topologies for supramolecular network crystals form, based on local rules based on packing and binding thermodynamics.

The essential elements of the mesoatomic growth model described here are predicated on the following propositions:

(1) The dominant pathway for network crystal formation is one where micellelike groups (mesoatoms) of chains break isotropic (i.e., spherical) symmetry into lower point group symmetry, with nonconvex shapes before, during, or upon assembly with other mesoatoms into crystals.

(2) The optimized packing of the nonconvex asymmetric mesoatoms derives from both covalentlike and van der Waals–like binding, which dictates the ultimate crystal space group symmetry and topology of the crystalline assembly.

(3) To a good approximation, the shape and packing characteristics of the primordial mesoatom adding to a crystal can be derived from the structure of its ultimate mature shape in the final crystalline state observed experimentally and computed theoretically.

Each of these propositions raises open questions for experimental and theoretical studies of actual supramolecular network assembly. In our analysis above, we restricted our focus to diblock copolymers, but the relevance of mesoatoms clearly extends to other macromolecular contexts where these or similar morphologies occur. We offer some brief comments about extensions of mesoatom concepts to other molecular architectures below.

The proposition that kinetically favored nonconvex mesoatom shapes template the assembly process may be reasonable on its face but raises several important questions, illustrated by the schematic shown Fig. 8. How much do the thermodynamic prerogatives of molecular groups, due to the balance of entropy and enthalpy within those groupings alone, select the complex nonconvex shapes and node functionality of the ultimate networks vs adopting those nonconvex shapes upon assembly into multimesoatomic clusters? The preshaping scenario suggests that it should be possible to identify some range of thermodynamic conditions where individual (isotropic) spherical micellar domains (near to but slightly above the critical aggregation conditions) break symmetry into the elementary trihedral, tetrahedral, and octahedral symmetries consistent with the mature mesoatoms of DG, DD, and DP, respectively. In the absence of strong thermodynamic forces to preshape mesoatoms, mesoatoms might instead break symmetry upon binding with other mesoatoms. More generally, even if primordial mesoatoms are partially preshaped by their internal packing thermodyanmics, one should expect at least some difference between the shape and symmetry characteristics of the primordial mesoatomic elements with respect to the ultimate mature bonded mesoatoms in the crystal. For example, as noted previously, mature DG atoms are chiral, and it is very plausible at this spontaneous chirality (in + vs − types) would emerge only at the stage of binding with other mesoatoms in a growing cluster. Certainly, the free energy calculations (e.g., self-consistent field theory) may explore the extent of and range of conditions where preshaping in micellarlike groups might become unstable to nonconvex shapes with the trihedral, tetrahedral, or octahedral symmetries of the cubic TPN phases. More generally, this question points to the need for experiments that capture primordial mesoatom shapes, as we discuss below.

We note that our primary heuristic for identifying which particular positions of the ultimate crystal correspond to kinetically favorable groupings is purely based on topological and symmetry grounds (i.e., subregions of domains with maximal point symmetry). There are likely many conditions for double networks with a kinetic bias for other groupings. For example, should thermodynamic conditions at which mesoatoms first aggregate favor surface contact of one domain over another (i.e., nonselective solvent), the addition differences in the relative surface exposures of A- or B-type domains could bias assembly toward other high-symmetry points. In Fig. 15, we show comparative renderings of the mesoatoms of DG based on both 16*b* and 16*a* Wyckoff positions of $Ia\bar{3}d$. These constructions exploit a more refined strong-segregation packing description [31] which includes distributions of chain trajectories modeled by prismatic wedges extracted from medial

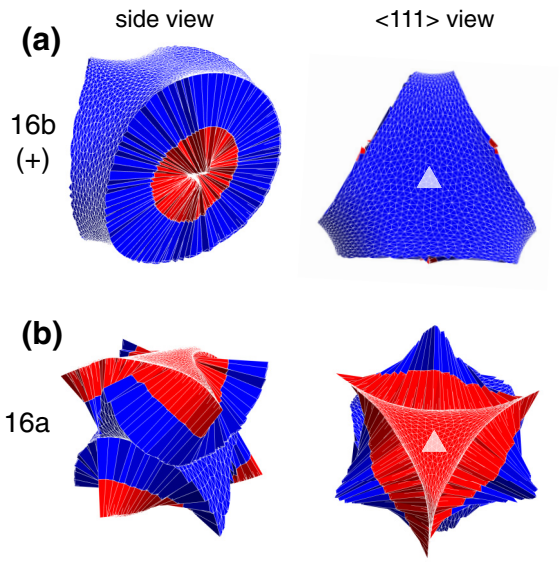

FIG. 15. Comparison of expected shapes of (a) 16*b* mesoatoms to (b) putative 16a mesoatoms based on the medial tessellations of the double gyroid (DG). Triangular prismatic regions model mean chain trajectories extending between terminal boundaries. While 16*b* mesoatoms are bound only by the triply-periodic minimal surface-like (outer) terminal surface of the matrix block, large fractions of 16*a* mesoatom surfaces are bound by weblike (inner) terminal surface of the tubular block. In the ⟨111⟩ view, only the threefold axis is highlighted of the respective D_3 (16*b*) and C_{3i} (16a) shown.

surfaces of gyroid surfaces that model the terminal boundaries in the matrix and tubular domains. In this case, we observe that the strut faces of the 16*b* mesoatom must be at least slightly nonplanar to avoid cutting chain trajectories. The shape of the 16*a* mesoatom is otherwise markedly different, in that its surface is not bound by the TPMS-like terminal boundary of the matrix domains but instead the twisted-web shape of the terminal surface of the inner domains, which closely approximates the inner medial surface of the IMDS. Because of more complex and disconnected geometry of these bounding terminal surfaces, the putative 16*a* mesoatom is clearly more complex in shape, with an even larger surface to interior volume ratio than the 16*b* position. Additionally, because it includes subdomain regions from each of the two gyroid networks, it possesses two disjoint regions of the IMDS, as opposed to the single IMDS patch of the 16*b* mesoatom. Presuming that thermodynamics of IMDS formation is dominant in the formation of primordial mesoatoms, this suggests that the 16*a* mesoatom type would require two IMDS nucleation events to form, as opposed to the single IMDS nucleation for the 16*b* mesoatom, and hence, kinetics of mesoatom formation of the 16*a* mesoatom (or any other mesoatom composed of fragments from multiple domains) would likely be much slower than the 16*b* mesoatom. However, it is possible that, under conditions where increased surface exposure of the minority domains is favorable over the majority domain, nucleation of 16*a*-type mesoatoms could preempt formation of the 16*b*-type mesoatoms. Notably, unlike the 16*b* mesoatoms, 16*a* positions are achiral and are not described by a tubular junction motif but instead a double-layer minimal saddle patch. While the shape and local contact of such a distinct domain will template altogether distinct assembly kinetics, it is straightforward to consider how to extend the analysis and arguments presented here to these alterative shape and symmetry mesoatoms.

The second and third propositions that packing the nonconvex mesoatomic shapes templates the ultimate crystal formation raise an important question about the malleability of mesoatoms. Mesoatomic groupings are composed of large numbers of flexible molecules. For example, in the DD and DG assemblies from polystyrene-b-polydimethylsiloxane (PS-PDMS) diblocks reported in Refs. [25,41], one can calculate that the respective tetrahedral and trihedral nodal volumes possess roughly 2500 and 1100 chains. Owing to their many mobile, flexible, and independent constituent parts, mesoatoms are inherently malleable objects, and the thermodynamics of their intermesoatomic packing takes place at a similar free energy scale to thermodynamics of their internal rearrangements. This means that mesoatomic shapes are far from static and likely evolve and adapt significantly during the binding event to a growing crystal. As alluded to above, binding along intranetwork struts by match-up of the respective block regions across the strut bond is likely to require some degree of radially combing chains along the normal to the skeletal graph at the endcaps of the primordial mesoatom (e.g., Fig. 15). It is also reasonable to expect the shape of the outer saddle skin of mesoatoms to adjust somewhat as opposing brushes come into close contact. Notably, for DG mesoatoms, there is an additional question about when and how primordial mesoatoms that compose the alternate + and − networks break achiral symmetry. One possibility (consistent with the assumptions of our minimal growth model) is that primordial mesoatoms themselves are unstable, spontaneously breaking symmetry into distinct populations of opposite chirality, and this preexisting chirality organizes the subsequent kinetics of crystal formation. An alternative scenario, arguably more plausible for achiral constituents, is that primordial mesoatoms of DG are achiral and become chiral upon binding and adapting to the intercatenating DG crystals. These effects all suggest a more realistic physical model of mesoatomic assembly will require malleability of the shapes and intermesoatom correlations, most crucially allowing bonding along different faces to take place over a more flexible range of angles and distances.

Several classes of discrete particle models have been developed in recent years that incorporate anisotropic binding directions and strengths, mimicking the key features of our mesoatomic particle model. These include models of convex hard polyhedra [42], whose complex shapes and symmetries lead to the formation of a rich array of crystalline and liquid crystalline morphologies, purely due to entropy and close-packing considerations (i.e., what has been dubbed entropic bonding [43]). Relative to such models, our description of mesoatom assembly assumes that binding is cohesive and likely more important and that the nesting of nonconvex particles is necessary to guide the formation of properly intercatenated double networks. Beyond such hard particle models, a range of patchy sphere models has been explored in the recent decades motivated by questions as broad as colloidal glass formation, functional DNA liquid assembly, and thermo-

dynamic anomalies of water [44–46]. These typically involve building short-ranged sticky patches on otherwise isotropic (spherical) cores [47], with a fixed number and symmetrical arrangements. Notably, these models parameterize a degree of angular fluctuation in the binding, which would serve as a proxy of mesoatomic malleability [48]. However, at present, most models include only attractions along strut directions of what might ultimately result as like-network contacts (e.g., only trivalent or tetravalent sticky bonds). Considering the above results, it would be interesting to understand how the incorporation of attractive interactions along directions that enable internetwork binding would influence the thermodynamics and kinetic accessibility of intercatenated double-network crystal formation. Lastly, we note the existence of network forming models where the local building blocks (i.e., the mesoatoms) of the crystals themselves are composed of at least a few distinct particles. The interactions between the components of those mesoatomic motifs both template the stable local symmetries of those units, as well as their flexibility and potential ability to reconfigure between different types of mesoatoms, much like what would be expected for supramolecular mesoatoms. Based on a binary mixture of two classes of attractive particles, Kumar and Molinero [49] and Marriott *et al.* [50] have developed and explored a model in which DG crystals compete with lamellar and columnar phases, leading to rich insights into phase formation, transformation pathways, nucleation, and growth of DG crystals [51]. A model of anisotropically sticky spheres developed by Morphew *et al.* [52] and Rao *et al.* [53] has been shown to exhibit assembly into tetravalent and hexavalent network crystals. However, at present, only single networks (e.g., single diamond [48]) have been observed in simulations of these models, presumably because the close packing of bound spherical cores obstructs the incorporation of a second intercatenated network. Certainly, generalization and extensions of such models as coarse-grained representations of mesoatoms hold potential for more extensive studies of equilibrium and nonequilibrium assembly from mesoatomic units. One challenge will be to parameterize the complex shapes, anisotropic binding, and deformability of these coarse-grained mesoatoms in terms of physical models that connect to intradomain deformation of supramolecular packing within those units.

The malleable nature of mesoatomic elements has important consequences not only for the fluctuations of local bonds/bond angles in growing crystals but even more profound consequences for the complex possibilities of distinct states of disorder or defects in network assemblies as well as pathways of interconversion from one type of network to another. Next, we describe this and other experimental implications for the putative mesoatomic building blocks of network crystals.

B. Experimental fingerprints of network mesoatoms

The conjectured notion that mesoatomic units extracted from the final ideal double-network crystals are the natural building blocks of these structures leads to two basic questions:

(1) Where, when, and how might mesoatomic assembly be observed?

(2) How might properties of malleable mesoatoms influence postassembly behavior and properties?

We first address the question of observing mesoatoms in the primordial state and their assembly. Crudely speaking, one can expect two classes of kinetic pathways where mesoatomic elements form: (1) mesoatom-first formation followed by mesoatomic aggregation into ordered structures and (2) spinodallike formation of randomly connected network-like domains, which later mature into ordered structures.

This first path (mesoatoms-first) suggests conditions at early times of an initially disordered (mixed) system, evolving into discrete primordial, micellelike groupings before their association into multimesoatom arrangements of the type that ultimately become ordered crystals. Primordial mesoatoms would be expected to form an initially homogeneous melt by cooling or from a homogeneous solution by solvent evaporation and may or may not necessarily adopt nonconvex, symmetry-broken states prior to assembly into clusters (e.g., Fig. 8). Processing routes that may give rise to mesoatom-first assembly are twofold. In a neat system (i.e., pure diblocks) near the binodal curve (but outside of the spinodal region), it may be possible to image the formation of primordial network mesoatoms that take the form of nonconvex micelles coexisting with disaggregated chains. Such is the natural picture for the disordered sphere phases that form at the high-χN and high-compositional asymmetry regime of diblocks but, for formation of mesoatoms of a tubular cubic phase, implies that chain compositions are likely closer to regimes favoring packing intermediate to lamellar or cylindrical morphologies, where the gap between binodal and spinodal regions is typically smaller. Therefore, a second processing route in which assembly is cast from a volatile solvent may be favorable for mesoatom-first assembly since it allows formation of primordial mesoatoms (with potentially complex shape) but at initially dilute conditions. However, as a two-component system, this processing route introduces the complexity that, as the solvent is evaporated, the appearance of a variety of mesoatoms and mesoatom aggregates would depend on the solvent concentration and solvent quality for each block, including the possibility for the formation of alternative mesoatoms leading to nonequilibrium, metastable phases.

Observing mesoatom-first assembly is challenging, as it requires both temporal resolution but also the ability to characterize low-symmetry shapes with complex features at the scale of few to tens of nanometers. In principle, time-resolved *in situ* scattering may be used to note the formation of some sort of transient features associated with the early stages of mesoatomic group formation prior to the onset of long-range order. This is the scenario described, for example, for time-resolved small angle x-ray scattering (SAXS) studies of solution-cast PS-PDMS assemblies [54], where scattering at intermediate times suggested the formation of some sort of aggregates without long-range order prior to the signal of established long-range order of the periodically ordered state (e.g., DG). However, in this and other cases with isotropically averaged scattering intensity, data are difficult if not impossible to interpret what the (likely polymorphic) 3D shapes are

that give rise to that scattering peak. This shortcoming then points to microscopy methods to observe mesoatoms in their primitive states to cast further light on how their shapes evolve upon fusion with a growing crystal.

In principle, electron microscopy (EM) experiments can reveal much more specific geometric detail for low-symmetry shapes of polymeric domains at the scales of putative mesoatom assembly pathways. However, such methods are traditionally limited to particular snapshots of arrested structures. For example, for solvent-cast systems, one might expect that cryo-EM is suitable to capture mesoatoms in their primitive states as well as complex geometries of multimesoatom assembly. Such an approach relies on controlled vitrification via rapid thermal quenching ($\sim 10^{10}$ K/s) of the solvent prior to imaging. Such studies have been applied to solvent surfactant systems to capture complex 3D morphologies, notably the disordered membrane structure formed in surfactant/water microemulsions, denoted as L3 or the sponge phase [55,56]. Research on the solution behavior of amphiphilic macromolecules [53,54] has adopted the same techniques for successful imaging of mesoatoms of spherical and cylindrical micelles [57] as well as for revealing nodal Y junctions between wormlike micelles [58]. Notably, these trivalent local regions share the same trihedral symmetry as the putative DG mesoatom and may indeed be precursors to spongy assemblies in polymeric surfactant assembly. A principal shortcoming of these cryo-EM-based approaches, for the purposes of monitoring evolution of mesoatomic assembly, is the lack of time resolution. Recently, variable temperature liquid cell (VTLC) sample holders for transmission electron microscopy (TEM) have been developed with thin, electron-transparent windows, enabling direct, real-time imaging of nanoscale assembly [59]. Korpanty *et al.* [60] made VTLC TEM measurements of transient intermediate structures from thermally induced rearrangement of the inner core region of ABC triblock spherical micelles, which when compared with changes in the form factor from variable temperature SAXS show good correspondence with changes in domain shape. Future application of VTLC and cryo-EM techniques for imaging the primordial mesoatoms in tubular network polymers seem very promising.

A second path (sponge-first) to forming TPN crystals is arguably simpler, which would follow from cooling a single component diblock from its high-temperature disordered near-homogeneous melt state to a temperature below the ODT where, over time, compositional fluctuations may lead to (nearly) spinodal decomposition into a disordered microphase separated state (sometimes also referred to as a sponge phase) which then evolves via nucleation and growth into the ordered crystal from the parent disordered network state. In this path, a stage where mesoatoms are observed as individual, disassembled units may not even exist, but nevertheless, we posit that the collective behavior of the system—most importantly, its longer-term evolution to an ordered structure—is likely to be controlled by the collective reconfiguration of these local groupings.

Capturing complex network assemblies in disordered arrangements has been previously accomplished by EM tomography (EMT), particularly in a diblock-homopolymer blend, resulting in a 3D reconstruction disordered networklike macromolecular sponge phase alongside ordered grains of

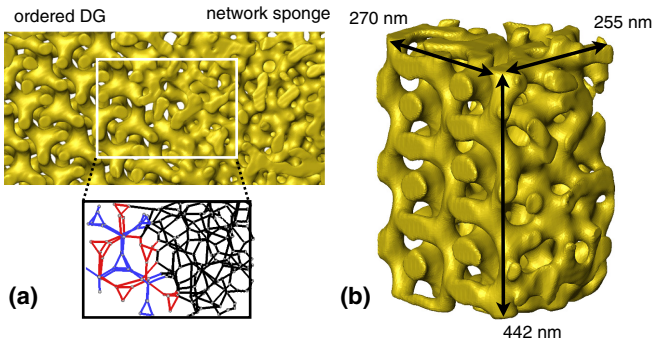

FIG. 16. Three-dimensional (3D) slice and view scanning electron microscopy tomography (SVSEMT) reconstruction of a region of a PS-PDMS diblock showing the boundary between a grain of the double-gyroid (DG) crystal with intercatenated trihedral networks (left) and a region of a spongelike phase (right). (a) Skeletonization of the highlighted subregion spanning the boundary the interface between ordered and random networks. Skeletal graph bonds are shown as red/blue on the alternating gyroids of DG, while the random network bonds (a single fused network) are shown as black. (b) Volume with spatial dimension for scale. Over 88% of the units in the disordered network are trihedral, with all mesoatom units belonging to a single network. (Figures courtesy W. Shan). Note: This sample is not from spinodal decomposition, rather rapid evaporation of a solution (e.g., Ref. [39]).

DG [56]. Detailed analysis of the skeletal axes of the tubular domains revealed that locally trihedral nodal regions dominate in the disordered sponge (89% of the nodes of the associated skeletal graph had 3 functionality) along with some small, perforated layerlike regions. Further analysis of regions where a growing DG cluster evolves from an adjacent disordered region would shed much light on possible mechanisms for the disordered-to-ordered phase transformation and the role of malleable mesoatoms (e.g., local rotations and relinking of trihedral nodal junctions at the crystal growth front). A relatively new electron microscope technique, slice and view scanning EMT (SVSEMT), provides systematic imaging of much greater regions than TEM of thin sections—indeed, many hundreds to tens of thousands of cubic micron volumes (containing $\sim$ 10 million unit cells) can be 3D reconstructed [41]. SVSEMT involves creating a series of images at different depths of a sample by using a low-voltage electron beam to image the near surface of the sample, followed by ion-beam milling to remove a thin ($\sim$3 nm) slice of the sample, repeated over and over to produce a high-fidelity 3D tomographic reconstruction with $\sim$10 nm feature resolution (see Fig. 16).

An interfacial region between the gyroid sponge phase and a DG grain is shown in Fig. 16 for a PS-PDMS diblock (for details of sample and methods, see Ref. [41]). The viewing direction of the reconstruction can be chosen based on software manipulation of the 3D data, and at the left is along the [111] direction of the DG grain. The intercatenated minority component PDMS networks are readily identified, and their topology and geometry can be quantified by skeletonization of the 3D reconstruction. Interestingly, skeletonization of the adjoining sponge phase shows that $\sim$90% of the nodes in a volume of 10^8 nm^3 are trihedral units. Analysis of the strut directions in the sponge phase gives a nearly isotropic distribution, while

as expected within the ordered grain, the struts are all well aligned along the ⟨110⟩ directions of the unit cell. Due to the orientational disorder, dihedral angles between adjacent nodes which are used to determine network chirality in the ordered DG phase have a near isotropic distribution in the sponge phase. Moreover, in the region examined, there are no discrete, nonnetwork PDMS regions; rather, the minority PDMS component forms a single continuous network but without loop intercatenation. This disordered network structure is not unlike the atomic-scale continuous random network (CRN) model previously proposed for amorphous semiconductors (i.e., at $f = 3$, amorphous arsenic would correspond to disordered DG, while at $f = 4$, amorphous silicon would correspond to a DD CRN).

How the sponge phase transforms into the DG crystal is, at present, unknown. The transformation likely involves local translation and rotation of the trihedral mesoatoms to create the correct saddle shapes for the outer terminal surface that can then nest against one another while directing strut orientations along ⟨110⟩ directions. However, the sponge network must be occasionally disrupted to split the single noncatenated network with its wide range of loop sizes into two independent, intercatenated, opposite chirality, 10-3 loop networks. If mesoatoms are indeed the key structural elements of network assembly, we posit that they are not only the building blocks of the assembly but also capture the relevant degrees of freedom for the disorder-to-ordered network transformation. Future work needs to address the details of the distributions of the strut-strut angles, the strut lengths, and strut directions as well as characterization of the loop distributions, topologies, and various types of network point defects (e.g., $f = 4$ and 5 nodes as well as network breaks) as the structure evolves across the interface from single disordered sponge network to ordered DG networks. Moreover, future studies may uncover properties of prototypical mesoatoms via direct experimental observation of statistically large ordered/disordered network assemblies, for example, by analyzing the spread of its characteristic features (i.e., distributions of strut-strut angles, strut lengths, mesoatom volume, IMDS curvature, and surface area, dihedral angles between a mesoatom with its linked neighbors as well as the partitioning of its outer terminal surfaces with the surrounding mesoatoms and specification of the type and number of contacting neighbors).

C. Learning about mesoatomic malleability from defects

Going beyond the formation of TPN crystals, we posit further that mesoatomic groupings also describe the fundamental excitations of the crystalline state, in the form of the various defects they support. Studying how the local symmetries of a crystal can be disrupted by various defects yet allow the distorted structure to accommodate into the surrounding crystal with an overall small strain field (and hence low energy) can give insight into how mesoatomic units can adapt to their surroundings, which itself reflects the combinations of thermodynamics of the interior chain packing within mesoatoms as well as the effects of intermesoatomic packing. Defect identification and classification in tubular network BCP crystals is a relatively recent endeavor [61–63]. Unlike defects in atomic crystals where the structure simply rearranges the

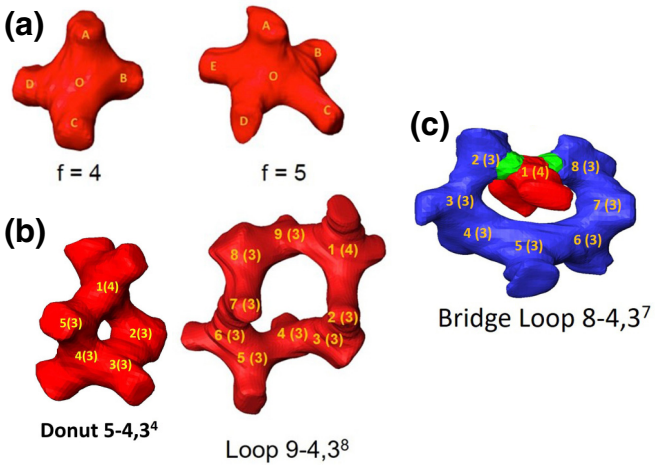

FIG. 17. Examples of the intermaterial dividing surface (IMDS) within mesoatom point defects occurring in an ordered double-gyroid (DG) grain. (a) Extracted defect mesoatoms with $f = 4$ and 5. (b) A functionality point defect having one or more extra struts necessitates changes to the network topology and new types of network circuits (donuts and loops) differing from the normal $10 - 3^{10}$ loop are formed. (c) A bridge defect occurs when the two networks fuse together. Reproduced from Ref. [64].

immutable atoms, in self-assembled crystals with malleable mesoatomic units, distortions and defects can and do strongly alter the shape and symmetry of the basic motif. Since defects disrupt the periodic packing scheme in the crystal, their presence influences both reciprocal-space data (scattering) and real-space data (microscopy). Therefore, as we have previously discussed, real-space analysis is necessary for detailed characterization. Next, we do a brief survey of defects with particular attention to how various defects in the DG phase create changes to the malleable $f = 3$ DG mesoatomic units.

Defects can be classified as point, line, or surface imperfections (zero-dimensional-, one-dimensional-, and 2D-type defects) that respectively break symmetry at a point or along a continuous curve or over a surface. Due to the mesoatoms forming a double intercatenated network structure, the notion of point defects needs to be extended to allow for somewhat larger motifs sometimes containing multiple mesoatomic units that together break symmetry in a local region (point) but allow rapid return of the structure to its ordered symmetries in adjacent regions. A variety of point defects in the DG phase were identified using SVSEMT [61]. These include node defects (so-called f defects), loops, and donuts as well as network-network bridges and network strut-break defects. Figure 17 shows a few examples of f, donut, loop, bridge, and break defects that are associated with various departures from the basic $f = 3$ mesoatom unit that is organized into $10 - 3^{10}$ intercatenated left- and right-handed chiral loops of the DG crystal. [The notation $X - Y^n$ here denotes a loop consisting of X nodes, each node has a functionality (valence) of Y, and there are n consecutive nodes circumventing the loop with this valence.] Analysis of the network topology of the DG revealed small, closed paths, denoted as donuts (e.g., a $5{-}4,\ 3^4$) that, due to the small diameter of the path, were not catenated, whereas larger loop paths containing

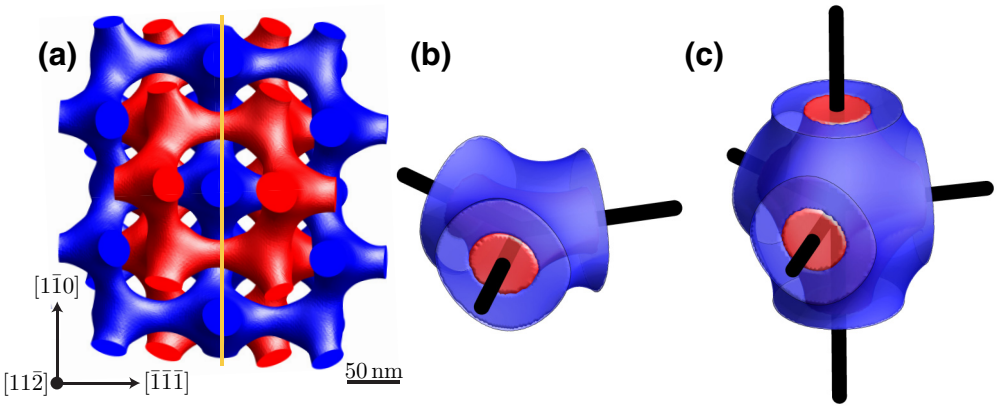

FIG. 18. A twin boundary defect (mirror plane indicated by the orange line) visualized by three-dimensional (3D) slice and view scanning electron microscopy tomography (SVSEMT) tomography of a PS-PMDS diblock creates two new types of double-diamond (DD) mesoatoms. (a) Experimental reconstruction of the (222) twin boundary in the DD phase as viewed along [112] (adapted from Ref. [62]). Two new types of mesoatoms having (b) $f = 3$ and (c) $f = 5$ are formed on the terminal boundary, both with D_{3h} point group symmetry instead of the T_d tetrahedral symmetry of normal DD mesoatoms. Experimental images courtesy of X. Feng and M. Dimitriyev.

multiple f defects were intercatenated (e.g., $9-4$, 3^2, 4, 3^5). In general, point defects are found to occur in small clusters such that, away from the cluster, the structure has returned to the normal crystalline ordered packing. These point defects in network phases exemplify the malleability of the mesoatoms (in this case, locally trihedral motifs like the 16*b* mesoatom of DG), with the ability of the motifs to adapt their local detailed shapes to maintain a smooth, continuous IMDS with relatively mild distortions of the minority and majority domain shapes and thicknesses to minimize the excess chain frustration that the defect(s) creates.

Dislocations are extended, generally 3D curved, line defects and break the translational symmetry of the crystal, around which the displacement slips by a net translation vector (called the Burgers vector) **b**. A recent TEMT study characterized a dislocation defect in the DG phase [65]. Due to the limited volume of the reconstruction only a relatively short (∼600 nm) length of dislocation could be investigated. Nevertheless, a dislocation line along [111] of mixed edge and screw character and a rather large Burgers vector $\mathbf{b} = a_o$ [012] could be clearly identified from the reconstruction. Surprisingly, the dislocation core did not exhibit any apparent new mesoatom features (e.g., nodal regions with other functionalities other than 3), although far-field compression away from the core apparently led to fusion/fission type point defects. Presumably, dislocations with different Burgers orientation and along different symmetry directions will in general require the formation of distinct mesoatoms, which do not appear as features of equilibrium, ideally ordered structures, but which do appear in recent studies of grain boundaries of DG and DD crystals.

Here, 2D surface defects (i.e., grain boundaries) occur due to impingement of neighboring grains during growth of the ordered phase, due to the misorientation of the lattices in the neighboring grains (i.e., tilt or twist). A twin boundary is a special type of tilt grain boundary where the boundary acts as a mirror plane for the adjacent grains. Twins are quite common low-energy defects in hard matter. Indeed, recently numerous twins have been found in both DG and DD phases [62,63]. Twins in the DG occur on (422) planes, and since the two networks are enantiomorphic, the twin acts as a topological mirror. The influence of the twin boundary on the mesoatom networks depends on if the nodes reside on the boundary or adjacent to the boundary. Three new types of achiral mesoatoms are created on the DG twin boundary as well as two new types of achiral loops. The IMDS is smooth and continuous across the twin boundary, and the new IMDS within the mesoatoms has similar mean and Gaussian curvatures as the normal IMDS within a 16*b* mesoatom, consistent with a low-energy defect.

Twins in the DD occur on (222) planes (see Fig. 18). Interestingly, in atomic diamond (the single-network structure of C, Si, Ge, etc.), twins occur on (111) planes. For the DD BCP network, the mesoatom network with its nodes offset from the boundary has the same structure as that of a twin in hard diamond where the struts (corresponding to the atomic bonds in diamond) connecting nodes on either side of the boundary are perpendicular to the boundary and retain their T_d symmetry. As was the case for the DG twin, the nodes of the second mesoatom network, which lie in the plane of the boundary and as such must exhibit mirror symmetry parallel to the boundary, transform to adopt D_{3h} symmetry [see Fig. 18(b)]. Twinning results in substantial modification of the normal mesoatom tetrahedral T_d point group symmetry to form two new types of mesoatoms (pentahedral $f = 5$ and trihedral $f = 3$) which both adopt D_{3h} symmetry. These mesoatoms alternate and link to form a hexagonal mesh comprised of $[6 - (5, 3)^3]$ loops in the plane of the boundary. Thus, the packing requirement of the mirror defect induces the mesoatomic point group symmetry to change from T_d to D_{3h}.

An additional key role for malleable mesoatoms lies with their contribution in order-order phase transformations in BCPs [28,66–69]. To convert from one phase with a particular space and point group symmetry mesoatom(s) to a second phase with a different space and point group symmetry mesoatom(s), the mesoatoms must undergo a size and shape transformation. In many studies, the new phase forms an epitaxial relationship with the existing phase that provides

a pathway for the transformation. Minimization of the disruptions to preferred packing on either side of the interphase boundary often results in a narrow transition zone across which the mesoatoms undergo restructuring, which implies the existence of new intermediate types of mesoatomic units.

D. Concluding remarks

We conclude with some brief remarks about basic challenges and questions opened by the mesoatomic concept when extended to chain architectures beyond the basic polymer amphiphile shape of linear AB diblock copolymers. Our simple mesoatom is defined by its inner terminal surface, the IMDS, and its outer terminal surface. Such discrete mesoatoms aggregate and pack via brush-brush interactions across the exposed terminal surfaces as well as linking and fusing of nearly parallel blocks across strut faces to smoothly extend the IMDS. Clearly, this mesoatom concept readily applies to tubular network forming AB diblock–homopolymer A or B blends—appropriately generalized to incorporate guest homopolymers in either the tubular or matrix domains. However, definition of the mesoatom of the AB diblock double network does not simply generalize to double networks formed by ABA triblocks (e.g., Refs. [70,71]), even of the same symmetry, since a portion of chain configurations bridge from one tubular network to the other spanning the midblock matrix [72]. For example, in DG, to dissect out the 16*b* mesoatoms (as argued for AB diblocks) from the final structure requires cutting bridging B chains to form the outer terminal mesoatom surface. In general, the presence of bridging blocks in the matrix phase that covalently connect two different IMDSs would then require the choice of a mesoatom with two IMDSs [i.e., mesoatom 16*a* in Fig. 15(b)]. A 3-subdomain, 2-IMDS mesoatom version of 16*a* would work for alternating ABC gyroids predicted and observed in linear ABC terblocks [73,74]. Moreover, in practice for terpolymers with three solvent-block interactions, it is very likely that, as solvent evaporates during the assembly, the shape and symmetry of the primordial mesoatoms evolve due to variations in the relative strength of enthalpic and entropic interactions as well as relative component volume fractions. Thus, the primordial dilute solution mesoatoms will likely evolve as the (necessarily preferential for 3 blocks) solvent evaporates, causing, for example, a primordial mesoatom initially comprised of 2 regions and 1 IMDS (say, an A domain+a solvent core region and an outer mixed B-C+higher solvent content region) to evolve during aggregation to demix the B and C blocks as solvent evaporates to create a new second IMDS between B and C as well as enabling the A and C blocks to link up to form tubular networks.

Beyond linear architectures, much more complex polycontinuous network topologies are predicted for ABC miktoarm stars, including extended and linked lines of periodically spaced triple junctions where all three domains meet [75,76]. Here, the constraint for all three blocks to covalently link at a single junction creates a new type of IMDS where the junctions are confined to parallel lines as opposed to spreading uniformly over surfaces [77]. Mesoatoms for star architectures will likely internally partition to reflect the relative volume fractions of each component and the cost of the various types of IMDSs between pairs of blocks, predicted to lead complex patterns of interwinding network domains, such as striped gyroids [76]. Whether a single generic set of rules can be constructed to divine mesoatomic shapes when accounting for the vast variations of nonlinear molecular architectures, interdomain topologies, and crystallographic (and potentially even quasicrystallographic) symmetries remains as a challenge. Clearly, the rich and ever-expanding palette of supramolecular chemistry demands improved understanding of how the molecules manage their local environments along the way from either the initial melt state or from the dilute solution state to the final ever-expanding suite of ordered morphologies.

ACKNOWLEDGMENTS

The authors are grateful to M. Dimitriyev, C. Burke, and W. Shan for stimulating discussions and valuable comments on this paper as well as M. Dimitriyev, X. Feng, and W. Shan for contributing figure elements. This paper was supported by the U.S. Department of Energy, Office of Basic Energy Sciences, Division of Materials Sciences and Engineering under Award No. DE-SC0022229.

[1] S. Hyde, S. Andersson, K. Larsson, Z. Blum, T. Landh, S. Lidin, and B. W. Ninham, *The Language of Shape: The Role of Curvature in Condensed Matter Physics, Chemistry, and Biology* (Elsevier, Amsterdam, 1997).

[2] F. S. Bates and G. H. Fredrickson, Block copolymer thermodynamics: Theory and experiment, Annu. Rev. Phys. Chem. **41**, 525 (1990).

[3] Z. Su, R. Zhang, X.-Y. Yan, Q.-Y. Guo, J. Huang, W. Shan, Y. Liu, T. Liu, M. Huang, and S. Z. D. Cheng, The role of architectural engineering in macromolecular self-assemblies via non-covalent interactions: A molecular LEGO approach, Prog. Polym. Sci. **103**, 101230 (2020).

[4] J. N. Israelachvili, Soft and biological structures, in *Intermolecular and Surface Forces*, 3rd ed. (Academic Press, Burlington, 2011), pp. 535–576.

[5] E. E. Dormidontova and T. P. Lodge, The order-disorder transition and the disordered micelle regime in sphere-forming block copolymer melts, Macromolecules **34**, 9143 (2001).

[6] G. M. Grason, Ordered phases of diblock copolymers in selective solvent, J. Chem. Phys. **126**, 114904 (2007).

[7] D. J. Mitchell, G. J. T. Tiddy, L. Waring, T. Bostock, and M. P. McDonald, Phase behaviour of polyoxyethylene surfactants with water. mesophase structures and partial miscibility (Cloud Points), J. Chem. Soc., Faraday Trans. 1 **79**, 975 (1983).

[8] P. Sakya, J. M. Seddon, R. H. Templer, R. J. Mirkin, and G. J. T. Tiddy, Micellar cubic phases and their structural relationships: The nonionic surfactant system $C_{12}EO_{12}$/water, Langmuir **13**, 3706 (1997).

[9] T. P. Lodge, B. Pudil, and K. J. Hanley, The full phase behavior for block copolymers in solvents of varying selectivity, Macromolecules **35**, 4707 (2002).

[10] H. Shin, M. J. Bowick, and X. Xing, Topological Defects in Spherical Nematics, Phys. Rev. Lett. **101**, 037802 (2008).

[11] E. L. Thomas, D. J. Kinning, D. B. Alward, and C. S. Henkee, Ordered packing arrangements of spherical micelles of diblock copolymers in two and three dimensions, Macromolecules **20**, 2934 (1987).

[12] J. Charvolin and J. F. Sadoc, Periodic systems of frustrated fluid films and ≪micellar≫ cubic structures in liquid crystals, J. Phys. France **49**, 521 (1988).

[13] G. Grason, The packing of soft materials: Molecular asymmetry, geometric frustration and optimal lattices in block copolymer melts, Phys. Rep. **433**, 1 (2006).

[14] S. Lee, C. Leighton, and F. S. Bates, Sphericity and symmetry breaking in the formation of Frank-Kasper phases from one component materials, Proc. Natl. Acad. Sci. USA **111**, 17723 (2014).

[15] M. Huang, C.-H. Hsu, J. Wang, S. Hei, X. Dong, Y. Li, M. Li, H. Liu, W. Zhang, T. Aida *et al.*, Selective assemblies of giant tetrahedra via precisely controlled positional interactions, Science **348**, 424 (2015).

[16] G. M. Grason, B. A. DiDonna, and R. D. Kamien, Geometric Theory of Diblock Copolymer Phases, Phys. Rev. Lett. **91**, 058304 (2003).

[17] A.-C. Shi, Frustration in block copolymer assemblies, J. Phys.: Condens. Matter **33**, 253001 (2021).

[18] K. D. Dorfman, Frank-Kasper phases in block polymers, Macromolecules **54**, 10251 (2021).

[19] Y. Liu, T. Liu, X.-Y. Yan, Q.-Y. Guo, J. Wang, R. Zhang, S. Shang, Z. Su, J. Huang, G.-X. Liu *et al.*, Mesoatom alloys via self-sorting approach of giant molecules blends, Giant **4**, 100031 (2020).

[20] A. Reddy, M. B. Buckley, A. Arora, F. S. Bates, K. D. Dorfman, and G. M. Grason, Stable Frank-Kasper phases of self-assembled, soft matter spheres, Proc. Natl. Acad. Sci. USA **115**, 10233 (2018).

[21] J. Charvolin and J. F. Sadoc, Periodic systems of frustrated fluid films and ≪bicontinuous≫ cubic structures in liquid crystals, J. Phys. France **48**, 1559 (1987).

[22] G. E. Schröder-Turk, A. Fogden, and S. T. Hyde, Bicontinuous geometries and molecular self-assembly: Comparison of local curvature and global packing variations in genus-three cubic, tetragonal and rhombohedral surfaces, Eur. Phys. J. B **54**, 509 (2006).

[23] E. L. Thomas, D. M. Anderson, C. S. Henkee, and D. Hoffman, Periodic area-minimizing surfaces in block copolymers, Nature (London) **334**, 598 (1988).

[24] M. W. Matsen, The standard Gaussian model for block copolymer melts, J. Phys.: Condens. Matter **14**, R21 (2002).

[25] A. Reddy, X. Feng, E. L. Thomas, and G. M. Grason, Block copolymers beneath the surface: Measuring and modeling complex morphology at the subdomain scale, Macromolecules **54**, 9223 (2021).

[26] M. J. Park, K. Char, J. Bang, and T. P. Lodge, Order-disorder transition and critical micelle temperature in concentrated block copolymer solutions, Macromolecules **38**, 2449 (2005).

[27] K. Kim, M. W. Schulze, A. Arora, R. M. Lewis, M. A. Hillmyer, K. D. Dorfman, and F. S. Bates, Thermal processing of diblock copolymer melts mimics metallurgy, Science **356**, 520 (2017).

[28] D. A. Hajduk, P. E. Harper, S. M. Gruner, C. C. Honeker, G. Kim, E. L. Thomas, and L. J. Fetters, The gyroid: A new equilibrium morphology in weakly segregated diblock copolymers, Macromolecules **27**, 4063 (1994).

[29] M. Schick, Avatars of the gyroid, Physica A **251**, 1 (1998).

[30] I. Prasad, H. Jinnai, R.-M. Ho, E. L. Thomas, and G. M. Grason, Anatomy of triply-periodic network assemblies: Characterizing skeletal and inter-domain surface geometry of block copolymer gyroids, Soft Matter **14**, 3612 (2018).

[31] A. Reddy, M. S. Dimitriyev, and G. M. Grason, Medial packing and elastic asymmetry stabilize the double-gyroid in block copolymers, Nat. Commun. **13**, 2629 (2022).

[32] G. E. Schröder-Turk, A. Fogden, and S. T. Hyde, Local v/a variations as a measure of structural packing frustration in bicontinuous mesophases, and geometric arguments for an alternating $Im\bar{3}m$ (I-WP) phase in block-copolymers with polydispersity, Eur. Phys. J. B **59**, 115 (2007).

[33] In general, the inner terminal surfaces are weblike structures that span the skeletal graphs [31], and while details of this shape have consequences for packing within double-network phases, they are less consequential for defining boundaries of their mesoatoms.

[34] A. H. Schoen, Reflections concerning triply-periodic minimal surfaces, Interface Focus. **2**, 658 (2012).

[35] P. D. Olmsted and S. T. Milner, Strong segregation theory of bicontinuous phases in block copolymers, Macromolecules **31**, 4011 (1998).

[36] P. J. F. Gandy, S. Bardhan, A. L. Mackay, and J. Klinowski, Nodal surface approximations to the P, G, D and I-WP triply periodic minimal surfaces, Chem. Phys. Lett. **336**, 187 (2001).

[37] M. Wohlgemuth, N. Yufa, J. Hoffman, and E. L. Thomas, Triply periodic bicontinuous cubic microdomain morphologies by symmetries, Macromolecules **34**, 6083 (2001).

[38] Wells describes these shortest network loops as 10-3 net, 6-4 net, and 4-6 net: A. F. Wells, *Three-Dimensional Nets and Polyhedra* (Wiley, New York, 1977).

[39] S. P. Gido and Z.-G. Wang, Interfacial curvature in graft and diblock copolymers and implications for long-range order in cylindrical morphologies, Macromolecules **30**, 6771 (1997).

[40] See Supplemental Material at http://link.aps.org/supplemental/10.1103/PhysRevMaterials.7.045603 for an animated sequence of the first 89 mesoatom additions in simulated growth of a DG crystal (solid mesoatoms on left and corresponding occupied skeletons on right).

[41] X. Feng, C. J. Burke, M. Zhuo, H. Guo, K. Yang, A. Reddy, I. Prasad, R.-M. Ho, A. Averopoulos, G. M. Grason *et al.*, Seeing mesoatomic distortions in soft-matter crystals of a double-gyroid block copolymer, Nature (London) **575**, 175 (2019).

[42] P. F. Damasceno, M. Engel, and S. C. Glotzer, Predictive self-assembly of polyhedra into complex structures, Science **337**, 453 (2012).

[43] E. S. Harper, G. van Anders, and S. C. Glotzer, The entropic bond in colloidal crystals, Proc. Natl. Acad. Sci. USA **116**, 16703 (2019).

[44] E. Bianchi, J. Largo, P. Tartaglia, E. Zaccarelli, and F. Sciortino, Phase Diagram of Patchy Colloids: Towards Empty Liquids, Phys. Rev. Lett. **97**, 168301 (2006).
[45] F. Sciortino and E. Zaccarelli, Reversible gels of patchy particles, Current Opinion Solid State Mater. Sci. **15**, 246 (2011).
[46] F. Smallenburg, L. Filion, and F. Sciortino, Erasing no-man's land by thermodynamically stabilizing the liquid-liquid transition in tetrahedral particles, Nature Phys **10**, 653 (2014).
[47] N. Kern and D. Frenkel, Fluid-fluid coexistence in colloidal systems with short-ranged strongly directional attraction, J. Chem. Phys. **118**, 9882 (2003).
[48] A. Neophytou, D. Chakrabarti, and F. Sciortino, Facile self-assembly of colloidal diamond from tetrahedral patchy particles via ring selection, Proc. Natl. Acad. Sci. USA **118**, e2109776118 (2021).
[49] A. Kumar and V. Molinero, Why is gyroid more difficult to nucleate from disordered liquids than lamellar and hexagonal mesophases? J. Phys. Chem. B **122**, 4758 (2018).
[50] M. Marriott, L. Lupi, A. Kumar, and V. Molinero, Following the nucleation pathway from disordered liquid to gyroid mesophase, J. Chem. Phys. **150**, 164902 (2019).
[51] A. J. Mukhtyar and F. A. Escobedo, Developing local order parameters for order-disorder transitions from particles to block copolymers: Methodological framework, Macromolecules **51**, 9769 (2018).
[52] D. Morphew, J. Shaw, C. Avins, and D. Chakrabarti, Programming hierarchical self-assembly of patchy particles into colloidal crystals via colloidal molecules, ACS Nano **12**, 2355 (2018).
[53] A. B. Rao, J. Shaw, A. Neophytou, D. Morphew, F. Sciortino, R. L. Johnston, and D. Chakrabarti, Leveraging hierarchical self-assembly pathways for realizing colloidal photonic crystals, ACS Nano **14**, 5348 (2020).
[54] T.-Y. Lo, C.-C. Chao, R.-M. Ho, P. Georgopanos, A. Avgeropoulos, and E. L. Thomas, Phase transitions of polystyrene-*b*-poly(dimethylsiloxane) in solvents of varying selectivity, Macromolecules **46**, 7513 (2013).
[55] A. L. Parry, P. H. H. Bomans, S. J. Holder, N. A. J. M. Sommerdijk, and S. C. G. Biagini, Cryo electron tomography reveals confined complex morphologies of tripeptide-containing amphiphilic double-comb diblock copolymers, Angew. Chem. Int. Ed. **47**, 8859 (2008).
[56] G. Porte, J. Marignan, P. Bassereau, and R. May, Shape transformations of the aggregates in dilute surfactant solutions: A small-angle neutron scattering study, J. Phys. France **49**, 511 (1988).
[57] Y.-Y. Won, A. K. Brannan, H. T. Davis, and F. S. Bates, Cryogenic transmission electron microscopy (Cryo-TEM) of micelles and vesicles formed in water by poly(ethylene oxide)-based block copolymers, J. Phys. Chem. B **106**, 3354 (2002).
[58] S. Jain and F. S. Bates, On the origins of morphological complexity in block copolymer surfactants, Science **300**, 460 (2003).
[59] G. M. Scheutz, M. A. Touve, A. S. Carlini, J. B. Garrison, K. Gnanasekaran, B. S. Sumerlin, and N. C. Gianneschi, Probing thermoresponsive polymerization-induced self-assembly with variable-temperature liquid-cell transmission electron microscopy, Matter **4**, 722 (2021).
[60] J. Korpanty, L. R. Parent, N. Hampu, S. Weigand, and N. C. Gianneschi, Thermoresponsive polymer assemblies via variable temperature liquid-phase transmission electron microscopy and small angle x-ray scattering, Nat. Commun. **12**, 6568 (2021).
[61] X. Feng, H. Guo, and E. L. Thomas, Topological defects in tubular network block copolymers, Polymer **168**, 44 (2019).
[62] X. Feng, M. Zhuo, H. Guo, and E. L. Thomas, Visualizing the double-gyroid twin, Proc. Natl. Acad. Sci. USA **118**, e2018977118 (2021).
[63] X. Feng, M. S. Dimitriyev, and E. L. Thomas, Soft, malleable double diamond twin, Proc. Natl. Acad. Sci. USA. **120**, e2213441120 (2023).
[64] H. Jinnai, H. Hasegawa, Y. Nishikawa, G. J. A. Sevink, M. B. Braunfeld, D. A. Agard, and R. J. Spontak, 3D nanometer-scale study of coexisting bicontinuous morphologies in a block copolymer/homopolymer blend, Macromol. Rapid Commun. **27**, 1424 (2006).
[65] T. Miyata, H.-F. Wang, T. Suenaga, D. Watanabe, H. Marubayashi, and H. Jinnai, Dislocation-induced defect formation in a double-gyroid network, Macromolecules **55**, 8143 (2022).
[66] D. A. Hajduk, R.-M. Ho, M. A. Hillmyer, F. S. Bates, and K. Almdal, Transition mechanisms for complex ordered phases in block copolymer melts, J. Phys. Chem. B **102**, 1356 (1998).
[67] M. W. Matsen, Cylinder ↔ Gyroid Epitaxial Transitions in Complex Polymeric Liquids, Phys. Rev. Lett. **80**, 4470 (1998).
[68] C.-Y. Wang and T. P. Lodge, Kinetics and mechanisms for the cylinder-to-gyroid transition in a block copolymer solution, Macromolecules **35**, 6997 (2002).
[69] J. Jung, J. Lee, H.-W. Park, T. Chang, H. Sugimori, and H. Jinnai, Epitaxial phase transition between double gyroid and cylinder phase in diblock copolymer thin film, Macromolecules **47**, 8761 (2014).
[70] A. Avgeropoulos, B. J. Dair, N. Hadjichristidis, and E. L. Thomas, Tricontinuous double gyroid cubic phase in triblock copolymers of the ABA type, Macromolecules **30**, 5634 (1997).
[71] H. Jinnai, Y. Nishikawa, R. J. Spontak, S. D. Smith, D. A. Agard, and T. Hashimoto, Direct Measurement of Interfacial Curvature Distributions in a Bicontinuous Block Copolymer Morphology, Phys. Rev. Lett. **84**, 518 (2000).
[72] M. W. Matsen and R. B. Thompson, Equilibrium behavior of symmetric ABA triblock copolymer melts, J. Chem. Phys. **111**, 7139 (1999).
[73] T. H. Epps, E. W. Cochran, T. S. Bailey, R. S. Waletzko, C. M. Hardy, and F. S. Bates, ordered network phases in linear poly(isoprene-*b*-styrene-*b*-ethylene oxide) triblock copolymers, Macromolecules **37**, 8325 (2004).
[74] J. Qin, F. S. Bates, and D. C. Morse, Phase behavior of non-frustrated ABC triblock copolymers: Weak and intermediate segregation, Macromolecules **43**, 5128 (2010).
[75] M. G. Fischer, L. de Campo, J. J. K. Kirkensgaard, S. T. Hyde, and G. E. Schröder-Turk, The tricontinuous 3ths(5) phase: A new morphology in copolymer melts, Macromolecules **47**, 7424 (2014).
[76] J. J. K. Kirkensgaard, M. E. Evans, L. de Campo, and S. T. Hyde, Hierarchical self-assembly of a striped gyroid formed by threaded chiral mesoscale networks, Proc. Natl. Acad. Sci. USA **111**, 1271 (2014).
[77] S. Okamoto, H. Hasegawa, T. Hashimoto, T. Fujimoto, H. Zhang, T. Kazama, A. Takano, and Y. Isono, Morphology of model three-component three-arm star-shaped copolymers, Polymer **38**, 5275 (1997).